Physics – Uspekhi **40** (5) 495 – 515 (1997)

REVIEWS OF TOPICAL PROBLEMS PACS numbers: **42.66.–p**, **87.56.–v**, **87.80.+s**

Light scattering study of tissues

V V Tuchin

Contents

Abstract. Tissue optics is a rapidly expanding field of great interest to those involved in the development of optical medical technologies. In the present review both strongly (multiple) scattering tissues, such as skin, brain tissues, and vessel walls, and weakly scattering high-transparent tissues, such as eye tissues (cornea and lens), are discussed. For the former, radiation transport theory or Monte Carlo simulation are used to describe the propagation of light (laser beams). For weakly scattering ordered tissues, ensembles of close-packed Rayleigh or Mie scatterers are employed. Methods for solving the inverse problem of finding biotissue optical parameters are discussed. The propagation of photon-density diffusion waves in scattering and absorbing media is analyzed and the prospects of these waves for optical tomography are discussed. Polarization phenomena in both strongly and weakly scattering biotissues are discussed.

1. Introduction

Many up-to-date medical technologies have been developed based on recent progress in physics including optics. An interesting example relevant to the topic of this review is provided by computer tomography [1, 2]. X-ray, MR, and positron-emission tomographic techniques are extensively used in high-resolution studies of both anatomical structures and local metabolic events. Another safe and technically simple tool currently in use is diffuse optical tomography [1 – 3].

V V Tuchin N G Chernyshevskiĭ Saratov State University, ul. Astrakhanskaya 83, 410026 Saratov, Russia
Tel. (7-845-2) 24-60-36; (7-845-2) 51-51-95, (7-845-2) 99-16-93
Fax (7-845-2) 24-04-46
E-mail: tuchin@scnit.saratov.su

Received 26 July 1996, revised 16 December 1996
Uspekhi Fizicheskikh Nauk **167** (5) 517 – 539 (1997)
Translated by Yu V Morozov; edited by M S Aksent'eva

In terms of optical properties, biotissues (including blood, lymph, and other biological fluids) can be categorized into two large classes: (1) strongly scattering (opaque) tissues such as skin, brain, vascular walls, blood, and sclera whose optical properties are fairly well described in the framework of a multiple scattering model for scalar waves propagating in randomly inhomogeneous absorption media and (2) weakly scattering (transparent) tissues such as the cornea and lens in the anterior eye chamber; their optical properties are described by a single (or low-step) scattering model of ordered media composed of close packed scatterers with absorption centers [1 – 15].

The scalar approximation is often insufficient especially for the description of transparent tissues. The vector nature of waves in a scattering medium manifests in the polarization of an initially unpolarized light beam or the depolarization of initially polarized light during propagation [3, 5 – 8, 16 – 21].

Problems of optical diagnosis and spectroscopy of biotissues are concerned with two radiation regimes: continuous and time-resolved [1 – 3, 10 – 13]. The latter is realized by means of the exposure of a scattering object to short laser pulses ($\tau \sim 10^{-9} - 10^{-11}$ s) and the subsequent recording of scattered broadened pulses (the so-called time-domain method) or by irradiation with modulated light in the frequency range 100 MHz to 10 GHz and recording the degree of modulation of scattered light intensity and the corresponding phase shift at modulation frequencies (the so-called frequency-domain or phase method). The time-resolved regime is based on the excitation of the photon-density wave spectrum in a strongly scattering medium which can be described in the framework of the non-stationary radiation transfer theory (RTT). The continuous radiation regime is described by the stationary RTT [1 – 3, 10 – 13].

The problem of coherence is also relevant to the discussion of interactions between light and biotissues (scattering media). It has two aspects. On the one hand, coherence is lost due to multiple light scattering in randomly inhomogeneous media. On the other hand, backscattered radiation may undergo amplification of a narrow coherent component identified by probing biotissues with an ultrashort laser

pulse [1, 3, 4, 22, 23]. Light coherence is of primary importance for the selection of photons undergoing zero or a small number of scattering events and also for obtaining speckle-modulated fields from singly or multiply scattering phase objects [1, 3, 4, 24, 25]. Such approaches are important for coherent tomography, diffractometry, holography, photon-correlation spectroscopy and speckle-interferometry of biotissues and fluxes of biological fluids [1, 3 – 5, 25 – 30].

In the near infrared (IR) spectral region, light penetrates biotissues to a few centimeters but undergoes marked scattering which makes it difficult to obtain distinct images of optical inhomogeneities resulting from pathological processes, e.g. tumorogenesis, a local increase in blood volume due to hemorrhage and growing microvessels. Therefore, optical tomography needs new methods for the selection of photons carrying the image in a strongly scattering medium [1 – 5].

Another important area in which deep tissue probing is practiced is reflecting spectroscopy, e.g. optical oximetry for the evaluation of the degree of hemoglobin oxygenation in working muscular tissue, the diseased neonatal brain or the active brain of adults [1 – 3].

The present review is first and foremost concerned with light-scattering techniques recently developed for quantitative studies of biotissues and optical cell ensembles. It discusses the results of theoretical and experimental investigations into photon transport in biotissues and describes methods for the solution of direct and inverse scattering problems for random media with multiple scattering and quasiordered media with single scattering, to model different types of tissue behavior. The theoretical consideration is based on the stationary and non-stationary radiation transfer theories for strongly scattering tissues, the Mie theory for transparent tissues, and the numerical Monte Carlo method employed for the solution of direct and inverse problems of photon transport in multilayer biotissues with complicated boundary conditions.

These are general approaches extensible to the examination of a large number of abiotic scattering media. It is worthwhile to note that many known methods of scattering media optics, e.g. the integrating sphere technique, were brought to perfection when used in biomedical research. Concurrently, new measuring systems and algorithms for the solution of inverse problems were developed, useful for scattering media optics in general. Moreover, the improvement of certain methods proved possible only because they were needed for biotissue studies; this is especially true of the diffuse photon-density waves method, which is promising for the examination of many physical systems: aqueous media, gels, foams, air, aerosols, etc.

2. Optical properties of biotissues with strong (multiple) scattering

2.1 Propagation of CW light in biotissues

Biological tissues are optically inhomogeneous absorption media whose average refractive index is higher than that of air. This accounts for the partial reflection of radiation at the tissue/air interface (Fresnel reflection) while the remaining part penetrates the bioobject. Multiple scattering and absorption are responsible for laser beam broadening and eventual decay as it travels through a biotissue whereas volume scattering is a major cause of the dispersion of a large fraction of radiation in the backward direction (backscattering). Cellular organelles such as mitochondria are the main scatterers in various biotissues.

Absorbed light is converted to heat and reradiated in the form of fluorescence; it is also consumed in photobiochemical reactions. The absorption spectrum depends on the type of predominant absorption centers and water content of biotissues (see Fig. 1). Absolute values of absorption coefficients for typical biotissues lie in the range 10^{-2} to 10^{4} cm^{1} [1 – 3, 6, 7, 10 – 14, 32 – 40]. In the UV and IR ($\lambda \geqslant 2$ μm) spectral regions, light is readily absorbed which accounts for the small contribution of scattering and inability of radiation to penetrate deep into biotissues (across one or more cell layers). Short-wave visible light penetrates typical biotissues as deep as 0.5 – 2.5 mm where upon it undergoes an *e*-fold decrease of intensity. In this case, both scattering and absorption occur, with 15 – 40% of the incident radiation being reflected. In the wavelength range 0.6 – 1.5 μm, scattering prevails over absorption, and light penetrates to a depth of 8 – 10 mm. Simultaneously, the intensity of the reflected radiation increases to 35 – 70% of the total incident light (due to backscattering).

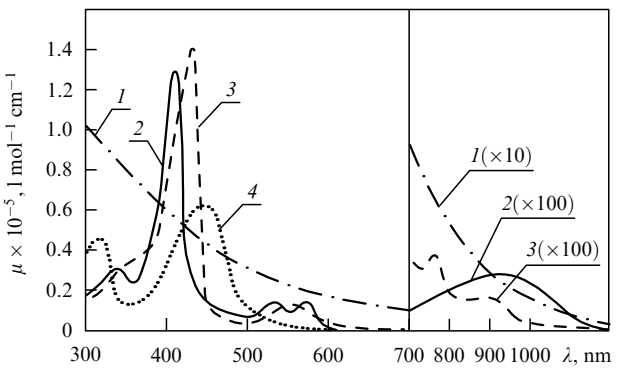

Figure 1. Molar attenuation spectra for solutions of main human skin pigments: *1* — DOPA-melanin (H_2O); *2* — oxyhemoglobin (H_2O), *3* — hemoglobin (H_2O); *4* — bilirubin ($CHC1_3$) [14].

Light interaction with a multilayer and multicomponent skin is a very complicated process [14]. The horny skin layer reflects about 5 – 7% of the incident light. A collimated light beam is transformed to a diffuse one by microscopic inhomogeneities at the air/horny layer interface. A major part of reflected light results from backscattering in different skin layers (horny layer, epidermis, dermis, microvessels). The absorption of diffuse light by skin pigments is a measure of bilirubin content, hemoglobin saturation with oxygen, and the concentration of pharmaceutical products in blood and tissues; these characteristics are widely used in the diagnosis of various diseases (see Fig. 1). Certain phototherapeutic modalities take advantage of ready transdermal penetration of visible and near IR light inside the body in the wavelength region corresponding to the so-called therapeutic window (0.6 – 1.5 μm). Solid tissues such as ribs and the cranium as well as whole blood are also easily penetrable for visible and near IR light [3, 7, 10]. Relatively good transparency of skin for longwave UV light (UV-A) depends on DNA, tryptophane, tyrosine, urocaninic acid, and melanin absorption spectra and underlies selected methods of photochemotherapy of skin tissues using UV-A irradiation [3, 6, 14].

A collimated (laser) beam dies away in a biotissue according to the exponential law

$$I(z) = (1 - R)\, I_0 \exp(-\mu_t z)\,, \tag{1}$$

where R is the coefficient of Fresnel reflection at the normal beam incidence, $R = [(n-1)/(n+1)]^2$, n is the relative refractive index, I_0 is the incident light intensity, $\mu_t = \mu_a + \mu_s$ is the extinction coefficient (interaction or attenuation coefficient), μ_a is the absorption coefficient, μ_s is the scattering coefficient, and z is the sample thickness. The mean free path of a singly scattered photon in a biotissue is denoted by $l_{ph} = \mu_t^{-1}$.

To analyse light propagation under multiple scattering conditions, it is assumed that absorbing and scattering centers are uniformly distributed across the tissue. UV-A, visible, or near IR radiation is normally subject to anisotropic scattering characterized by a well-apparent direction of photons undergoing single scattering which may be due to the presence of large cellular organelles (mitochondria, lysosomes, and inner membranes (Golgi apparatus) [10, 31]).

A sufficiently strict mathematical description of CW light propagation in a scattering medium is possible in the framework of the stationary RTT. This theory is valid for an ensemble of scatterers located far from one another and has been successfully used to work out some practical aspects of biotissue optics. The main stationary equation of RTT for monochromatic light has the form [1, 3, 10–14, 41, 42]:

$$\frac{\partial I(r,s)}{\partial s} = -\mu_t I(r,s) + \frac{\mu_s}{4\pi} \cdot \int_{4\pi} I(r,s')\, p(s,s')\, d\Omega'\,, \tag{2}$$

where $I(r,s)$ is the radiation intensity at a point r in the direction s, (W m^{-2} sr^{-1}); $p(s,s')$ is the scattering phase function, $d\Omega'$ is the unit solid angle in the direction s', and $\mu_s/\mu_t \equiv \Lambda$ is the albedo of single scattering. It is assumed that there are no radiation sources inside the medium.

If radiation transfer is examined in the $G \subset R^3$ range and ∂G is its boundary, then the boundary conditions can be written in the following general form [43]:

$$I(r,s)|_{(sn)<0} = S(r,s) + \widehat{R} I(r,s)|_{(sn)>0}\,, \tag{3}$$

where $r \in \partial G$, n is the external normal to ∂G, $S(r,s)$ is the radiation intensity of incident light, and $\widehat{R}$ is the reflection operator. When both absorption and reflection surfaces are present in the region G, conditions analogous to (3) must be given at each surface.

For practical purposes, integrals of the function $I(r,s)$ over certain phase space regions (r,s) are of greater value than the function itself. Specifically, optical probing of biotissues frequently measures the outgoing light distribution function at the medium surface $\Phi(r)$

$$\Phi(r) = \int_{(sn)>0} I(r,s)(sn)\, d\Omega\,, \tag{4}$$

where $r \in \partial G$. In problems of optical radiation dosimetry in biotissues, the measured quantity is actually the total radiant energy fluence rate at a point $U(r)$:

$$U(r) = \int_{4\pi} I(r,s)\, d\Omega\,. \tag{5}$$

The phase function $p(s,s')$ describes the scattering properties of the medium and is in fact the probability density function for scattering in the direction s' of a photon travelling in the direction s; in other words, it characterizes an elementary scattering act. If scattering is symmetric relative to the direction of the incident wave, then the phase function depends only on the angle θ between directions s and s', i.e.

$$p(s,s') = p(\theta)\,.$$

The assumption of random distribution of scatterers in a medium (i.e. the absence of spatial correlation in the biotissue structure) leads to normalization

$$\int_0^\pi p(\theta)\, 2\pi \sin\theta\, d\theta = 1\,.$$

In practice, the phase function is usually well approximated with the aid of the postulated Henyey–Greenstein function [1, 3, 10–14, 21]:

$$p(\theta) = \frac{1}{4\pi} \frac{1 - g^2}{(1 + g^2 - 2g\cos\theta)^{3/2}}\,, \tag{6}$$

where g is the mean cosine of the scattering angle θ (scattering anisotropy parameter)

$$g = \langle \cos\theta \rangle = \int_0^\pi p(\theta) \cos\theta 2\pi \sin\theta\, d\theta\,. \tag{7}$$

The value of g varies in the range from 0 to 1: $g = 0$ corresponds to isotropic (Rayleigh) scattering and $g = 1$ to total forward scattering (Mie scattering at large particles [21]).

The integro-differential equation (2) is too complicated to be employed for the analysis of light propagation in scattering media. Therefore, it is frequently simplified by representing the solution in the form of spherical harmonics. Such simplification leads to a system of $(N+1)^2$ connected differential partial derivative equations known as the P_N approximation. This system is reducible to a single differential equation of order $(N+1)$. For example, four connected differential equations reducible to a signle diffusion-type equation are necessary for $N = 1$ [44–50]. It has the following form for an isotropic medium:

$$(\nabla^2 - \mu_d^2)\, U(r) = -Q(r)\,, \tag{8}$$

where $\mu_d = [3\mu_a(\mu_a + \mu_s')]^{1/2}$ is the diffusion coefficient, $Q(r) = D^{-1} q(r)$, $q(r)$ is the source function (i.e. the number of photons injected into the unit volume), $D = c[3(\mu_a + \mu_s')]^{-1}$ is the photon diffusion coefficient, $\mu_s' = (1 - g)\,\mu_s$ is the reduced (transport) scattering coefficient, and c is the velocity of light in the medium. The transport mean path of a photon is $l_\delta = (\mu_a + \mu_s')^{-1}$. It is worthwhile to note that the transport mean path in a medium with anisotropic single scattering significantly exceeds the free path in a medium with isotropic single scattering $l_\delta \gg l_{ph}$ (see (1)). The transport path l_δ is the distance over which the photon loses its initial direction.

The diffusion theory provides a good approximation in the case of small scattering anisotropy factor $g \leqslant 0.1$ and large albedo $\Lambda \to 1$. For many tissues, $g \approx 0.6$–0.9, and can be as large as 0.995 for blood [34]. This significantly restricts the applicability of the diffusion approximation. It is argued that this approximation can be used at $g < 0.9$, when the optical thickness of an object is of the order

$\tau = \int_0^s \mu_t \, ds = 10 - 20$. However, the diffusion approximation is inapplicable for an input beam near the object's surface where single or low-step scattering prevails.

Now, let us briefly review other solutions of the transport equation. The so-called first order solution is realized for optically thin and weakly scattering media ($\tau < 1$, $\Lambda < 0.5$) when the intensity of a transmitting (coherent) wave is described by relation (1) or a similar expression [44]. Given a narrow beam (e.g. a laser), this approximation may be applied to denser tissues ($\tau > 1$, $\Lambda < 0.9$). However, certain tissues have $\Lambda \approx 1$ in the therapeutic window range which makes the first order approximation inapplicable even at $\tau \ll 1$.

A more strict solution of the transport equation is possible by the discrete ordinates method (multiflux theory) in which Eqn (2) is converted into a matrix differential equation for the illumination along many discrete directions (angles) [42]. The solution approximates an exact one as the number of angles increases. It has been shown in a previous paragraph that fluence rate is possible to expand in powers of spherical harmonics, separating the transport equation into the components for spherical harmonics. This approach also leads to an exact solution provided the number of spherical harmonics is sufficiently large. For example, a study of biotissues [51] made use of up to 150 spherical harmonics, and the resulting equations were solved by the finite differences method [52]. However, this approach requires tiresome calculations if a sufficiently exact solution is to be obtained. Moreover, it is hardly suitable for δ-shaped phase scattering functions [44].

Biotissue optics extensively employs simpler methods for the solution of transport equations, e.g. the two-flux Kubelka – Munk theory or three, four, and seven-flux models. Such representations are natural and very fruitful for laser tissue probing. Specifically, the four-flux model [42, 53] is actually two diffuse fluxes travelling to meet each other (Kubelka – Munk model) and two collimated laser beams, the incident one and the one reflected from the rear boundary of the sample. The seven-flux model is the simplest three-dimensional representation of scattered radiation and an incident laser beam in a semi-infinite medium [32]. Of course, the simplicity and the possibility of expeditious calculation of the radiation dose or rapid determination of tissue optical parameters (solution of the inverse scattering problem) is achieved at the expense of accuracy.

The development of new methods for the solution of direct and inverse radiation transfer problems for media with arbitrary configurations and boundary conditions is crucial for the reliable layer-by-layer measurements of laser radiation inside biotissues necessary for practical purposes including diffuse optical tomography and the spectroscopy of biological objects. The Monte Carlo (MC) method appears to be especially promising in this context, being widely used for the numerical solution of the RTT equation [54, 55] in different fields of knowledge (astrophysics, atmosphere and ocean optics, etc). It has recently been applied to biotissue optics [1 – 3, 13, 33, 35, 40, 53, 56 – 71]. The method is based on the numerical simulation of photon transport in scattering media. Random migrations of photons inside a sample can be traced from their input till absorption or output. Known algorithms allow a few biotissue layers with different optical properties to be characterized along with the final incident beam size and the reflection of light at interfaces. Typical examples of multilayer biotissues are skin, vascular, urinary bladder, and uterine walls.

For all its high accuracy and universal applicability, the MC method has one major drawback which is that it consumes too much machine time. Although advanced computer facilities and software systems diminish the role of time-factor, further developments in laser diagnostic and therapeutic tools require more effective, relatively simple and reliable algorithms of the MC method. For instance, the condensed MC method allows us to obtain the solution for any albedo, based on the results of modeling a single albedo which substantially facilitates computation [59]. Also, the development of very economical hybrid models currently underway is intended to combine the accuracy of the MC method and the high performance of diffusion theories or approximating analytic expressions [60, 61, 63].

Let us consider human skin optics as an example [14, 53, 58, 64 – 77]. In order to calculate light distributions $\Phi(r)$ and $U(r)$ by the MC method [see (4) and (5)], let us represent the skin as a plane multilayer scattering and absorbing medium (Fig. 2), with a laser beam falling normally onto its surface. Let us further assume that each i-th layer is characterized by the following parameters: μ_{ai}, μ_{si}, $p_i(\theta)$, the thickness d_i, and the refractive index of the filler medium n_i.

Using the MC algorithm described in [53, 58] to simulate the skin distribution of light beams with a Gaussian and flat profiles (see Fig. 2 and Table 1), the total fluence rate in the wavelength spectral regions 633 and 337 nm was obtained as shown in Fig. 3, along with the dependences of the maximum fluence rate U_m and the maximum fluence rate area D_m (determined from the $1/e^2$ level) on the incident beam radius for the wavelength of 633 nm (Fig. 4). It is readily seen that the illumination maximum is formed at a certain depth inside the tissue, and the total fluence rate at the point of maximum U_m may be significantly higher than that in the middle of the beam incident onto the surface of the medium (U_0). This was noticed by many authors (see for instance [1, 3]) who emphasized the strong correlation between the U_m/U_0 ratio

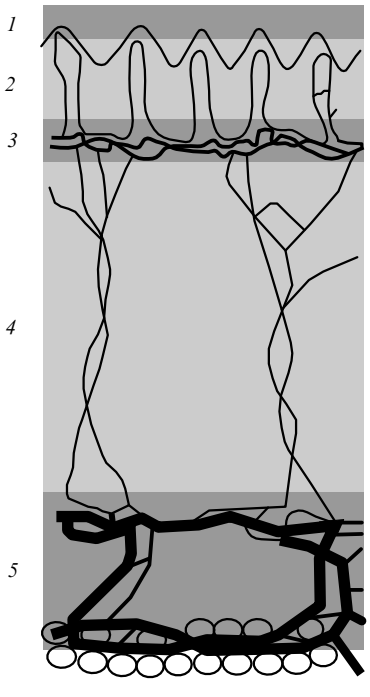

Figure 2. A model of skin: *1* — epidermis; *2* — dermis, *3* — dermis with *plexus superficialis* ; *4* — dermis; *5* — dermis *plexus profundus* [53].

Table 1. Optical parameters of skin: nominator $\lambda = 633$ nm, denominator $\lambda = 337$ nm [53].

No	Layer	μ_a, cm^{-1}	μ_s, cm^{-1}	g	n	d, μm
1	Epidermis	4.3/32	107/165	0.79/0.72	1.5	100
2	Dermis	2.7/23	187/227	0.82/0.72	1.4	200
3	Dermis with *plexus superficialis*	3.3/40	192/246	0.82/0.72	1.4	200
4	Dermis	2.7/23	187/227	0.82/0.72	1.4	900
5	Dermis *plexus profundus*	3.4/46	194/253	0.82/0.72	1.4	600

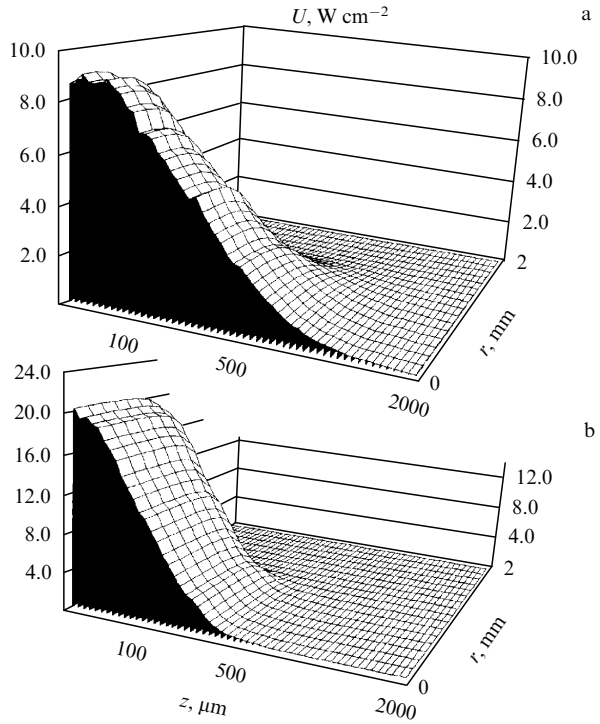

Figure 3. Results of Monte Carlo simulation of intensity distribution ($W\,cm^2$) in the skin irradiated by laser beams with Gaussian ($r_0 = 0.5$ mm, $\lambda = 633$ nm, $P = 25$ mW) (a) and flat ($r_0 = 0.5$ mm, $\lambda = 337$ nm, $P = 120$ mW) profiles [53].

and the optical properties of the medium, the incident beam radius, and boundary properties. It appears from Fig. 4b that an increase in the incident beam radius leads to a broadening of the illuminated area inside the tissue, with the enhancement rate in the transversal direction exceeding that along the beam.

For practical purposes, such calculations are necessary to correctly choose the irradiation doses for photochemical, photodynamic, and photohyperthermal therapy of oncological and many other diseases and the laser coagulation of surface blood vessels [3, 4, 6, 10–12, 14, 15, 33, 35, 38–40, 74–79].

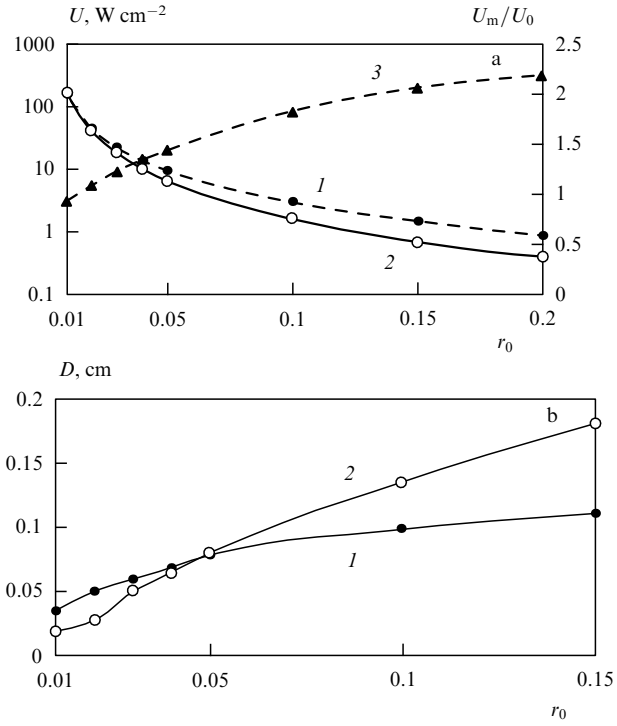

Figure 4. Parameters of the maximum illumination area as functions of the incident beam radius. A beam with a Gaussian profile, wavelength 633 nm, power 25 mW. *1* — total illumination in the centre of the incident beam U_0, *2* — maximal total illumination, *3* — U_m/U_0 (a); *1* — the size of the maximally illuminated area (at the $1/e^2$ level) along the beam axis, *2* — the size of the maximally illuminated area (at the $1/e^2$ level) normal to the beam axis [53].

2.2 Methods for the measurement of the optical parameters of biotissues

Methods for determining the optical parameters of biotissues can be divided into two large groups (direct and indirect methods) [1–3, 6, 7, 10–14, 32–40, 53, 59, 64–71, 80–103]. Direct methods include those based on some fundamental concepts and rules such as the Bougier–Beer law [see (1)], the single scattering phase function [see (6)] for thin samples, or the effective light penetration depth for slabs. The parameters measured are the collimated light transmission and the scattering indicatrix for thin samples or the fluence rate inside a slab. These methods are advantageous in that they use very simple analytic expressions for data processing. Their disadvantages are related to the necessity to strictly fulfill experimental conditions dictated by the selected model (single scattering in thin samples, exclusion of the effects of light polarization and refraction at cuvette edges, etc; in the case of slabs with multiple scattering, the recording detector (usually, a fiber lightguide with an isotropically scattering ball at the tip-end) must be placed far from both the light source and the medium boundaries.

Indirect methods imply the solution of the inverse scattering problem using a theoretical model of light propagation in a medium. They are in turn divided into iterational and non-iterational models. The former use equations in which the optical properties are defined through parameters directly related to the quantities being evaluated. The latter are based on the Kubelka–Munk model and multiflux models [32, 42, 44, 53, 80, 81, 97]. In indirect iterational methods, the optical properties are implicitly defined through measured para-

meters. Quantities determining the optical properties of a scattering medium are enumerated until the estimated and measured values for reflectance and transmittance coincide with the desired accuracy. These methods are cumbersome, but the optical models currently in use may be even more complicated than those underlying non-iterational methods (examples include the diffusion theory [42, 80, 99], inverse adding-doubling [88] and inverse MC (IMC) [53, 59, 85, 87, 90, 91,100] methods.

The optical parameters of biotissue samples (μ_a, μ_s and g) are measured by different methods. *In vitro* evaluation is most often achieved by the double integrating sphere method combined with collimated transmittance measurements. This approach implies either sequential or simultaneous determination of three parameters: collimated transmittance, diffuse transmittance T_d, and diffuse reflectance R_d. The optical parameters of the tissue are deduced from these measurements using different theoretical expressions or numerical methods (two and multiflux models, the IMC method) relating μ_a, μ_s and g to the parameters being investigated. In the simplest case, the two-flux Kubelka – Munk method is employed which is based on the relations presented in [64, 80]. μ_t is determined from collimated transmittance values based on relation (1) which allows all 3 parameters (μ_a, μ_s, g) to be found from the experimental data for T_d and R_d.

Any three measurements from the following five are sufficient for the evaluation of all 3 optical parameters [80]: the total (or diffuse) transmittance for collimated or diffuse radiation, the total (or diffuse) reflectance for collimated or diffuse radiation, the absorption by the sample placed inside an integrating sphere, the collimated transmittance (of unscattered light), or the angular distribution of radiation scattered by the sample.

Iterational methods normally take into account discrepancies between refractive indices at sample boundaries as well as the multilayer nature of the sample. The following factors are responsible for the errors in the estimated values of optical coefficients and need to be borne in mind in the comparative analysis of optical parameters obtained by different authors [80]: the physiological conditions of biotissues (the degree of hydration, homogeneity, species – specific variability, frozen/thawed or fixed/unfixed state, *in vitro*/*in vivo* measurements, smooth/rough surface), the geometry of irradiation, the matching/mismatching interface refractive indices, the orientation of detecting optical fibers inside the sample relative to the source lightguide, the numerical aperture of the recording lightguides, the angular resolution of photodetectors, the separation of radiation experiencing forward scattering from unscattered radiation, the theory used to solve the inverse problem.

The use of one of the measuring modalities in question can be illustrated by determining the optical parameters of human skin epidermis. Transmittance and reflectance spectra of thin epidermis slices (strippings (20 – 50 μm) measured in the wavelength range of 240 – 400 nm on a spectrophotometer with an integrating sphere were used to calculate the absorption $\mu_a(\lambda)$ and scattering $\mu_s(\lambda)$ coefficients based on a four-flux model taking into consideration collimated reflection at the sample boundaries [53, 69] (see Fig. 5). The differences between the absorption coefficients in the above wavelength range for normal human epidermis and samples containing psoriatic nidi are due to variations in skin metabolism. The epidermis of psoriatic skin is characterized by a marked

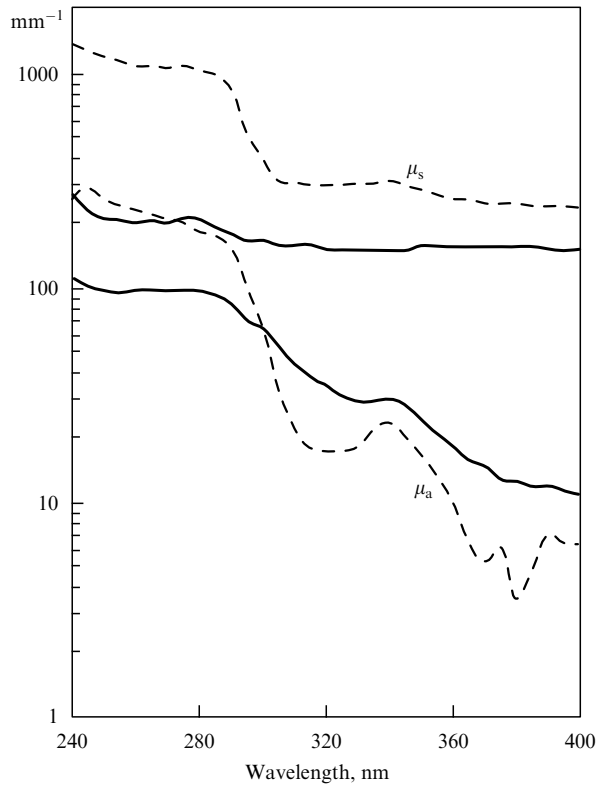

Figure 5. Calculated spectra for the absorption (μ_a) and scattering (μ_s) coefficients derived from experimental transmittance and diffuse reflectance spectra of human epidermis stripping using the four-flux model. Solid lines — normal skin, dotted lines — psoriatic skin [53, 69].

optical inhomogeneity caused by structural changes of the tissue in the psoriatic nidi and the appearance of air-filled microspaces between parakeratotic scales accounting for a 10 – 15% rise in the diffuse reflection coefficient (for strippings of normal epidermis, this coefficient at 240 – 400 nm increases by 6 – 10% at most).

The inverse adding – doubling (IAD) method provides a tool for the rapid and accurate solution of inverse scattering problems [88]. It is based on the general method for the solution of the transport equation for plane-parallel layers suggested by van de Hulst [98]. An important advantage of the IAD method when applied to biotissue optics problems is the possibility of rapidly obtaining iterational solutions with the aid of up-to-date microcomputers; moreover, it is flexible enough to take into account anisotropy of scattering and the internal reflection from the sample boundaries. The method includes the following steps: (1) the choice of optical parameters to be measured, (2) counting reflections and transmissions, (3) comparison of calculated and measured reflectance and transmittance, (4) repetition of the procedure until the estimated and measured values coincide with the desired accuracy.

In principle, the method allows for any intended accuracy to be achieved for all the parameters being measured provided the necessary computer time is available. An error of 3% or below is considered acceptable [88]. Also, the method may be used to directly correct experimental findings obtained with the aid of integrating spheres. The term 'doubling' in the name of the method means that the reflection and transmission estimates for a layer at certain ingoing and outgoing light angles may be used to calculate both the transmittance and

reflectance for a layer twice as thick by means of superimposing one upon the other and summing the contributions of each layer to the total reflectance and transmittance. Reflection and transmission in a layer having an arbitrary thickness are calculated in consecutive order, first for the thin layer with the same optical characteristics (single scattering), then by consecutive doubling of the thickness, for any selected layer. The term 'adding' indicates that the doubling procedure may be extended to heterogeneous layers for modeling multilayer biotissues or taking into account internal reflections related to sharp changes in refractive indices [88]. The IAD method has been successfully applied to determine optical parameters of human dermis (see [53, 71]).

Both the real geometry of the experiment and the biotissue structure may be complicated. Therefore, the MC method should be used if reliable estimates are to be obtained. However, the first algorithms to realize the IMC method became available quite recently [53, 85, 87, 90, 91, 100]. Refs [53, 85, 91, 100] report algorithms for the solution of similar problems by determining all three optical parameters of the biotissue (μ_a, μ_s and g) based on the *in vitro* evaluation of the total transmittance, diffuse reflectance, and collimated transmittance (for optically thin samples) using a spectrophotometer with integrating spheres. The initial approximation (to speed up the procedure) was achieved with the help of the Kubelka – Munk theory, specifically its four-flux variant [53, 91]. Both algorithms take into consideration the sideways loss of photons which becomes essential in sufficiently thick samples. Similar results were obtained using the condensed IMC method [59, 71].

μ_a, μ_s, and g values for the human brain, canine prostate, and porcine liver at 800 and 1064 nm as well as μ_a and μ_s spectra at 350 – 1050 nm for some strongly scattering eye tissues (sclera, retina) obtained by the IMC method from *in vitro* reflection and transmission measurements have been reported in [85, 100]. It is worthy of note that stable operation of the algorithm was maintained by generation of 10^5 – 5×10^5 photons per iteration. Two to five iterations were usually necessary to estimate the optical parameters with approximately 2% accuracy.

The required computer time can be diminished not only by the condensed IMC method but also by means of graphical solutions of the inverse problem following a preliminary MC simulation [87].

Also, the solution of the inverse problem by the MC method is possible in the framework of other measuring systems. For example, the authors of Ref. [90] studied the intensity distribution parameters of radiation transmitted through a biotissue (halfwidth, etc) while the condensed IMC method was employed in Ref. [71] to process *in vivo* estimates of radiation reflected from a biotissue which were obtained with the aid of a special sensor consisting of two photodiodes (660 and 940 nm) and three spaced photodetectors. *In vivo* μ_a and μ_s' values for human skin proved to be significantly smaller than those obtained *in vitro* (10 and 2 times respectively) [71]. For μ_a, the discrepancy may be attributed to the low sensitivity of the integrating sphere method at weak absorption combined with strong scattering ($\mu_a \ll \mu_s$); for μ_s', the discrepancy is related to the strong dependence of the method on variations of relative refractive indices for scatterers and the base medium of the tissue n, $\mu_s' \sim (n-1)^m$, $m \geqslant 2$ [71, 104].

Direct measurement of the scattering phase function $p(\theta)$ is important for the choice of an adequate model for the biotissue being examined [105]. The scattering phase function is usually determined from goniophotometric measurements in relatively thin tissue samples [32, 34, 53, 64 – 71, 92 – 94, 105, 106]. The scattering indicatrix measured with due regard for the geometry of the sample and experimental set-up is approximated either by the Henyey – Greenstein (HG) function (6) [53, 94, 105] or by a set of HG functions each characterizing the type of scatterers and specific contribution to the indicatrix [92]. In the limiting case of a two-component model of a medium containing large and small (compared with the wavelength) scatterers, the indicatrix is represented in the form of anisotropic and isotropic components [32, 71, 93]. Other approximating functions are equally useful, e.g. those obtained from the Rayleigh – Ganz approximation or ensuing from the exact Mie theory [89]. Such approximations were used to find the dependence of the scattering anisotropy factor g for dermis and epidermis on the wavelength in the range 300 to 1300 nm which proved to coincide fairly well with the empirical formula [64]

$$g_e \sim g_d \sim 0{,}62 + \lambda \cdot 0{,}29 \times 10^{-3} \ (\lambda, \ \text{nm}) . \tag{9}$$

on the assumption of a 10% contribution of isotropic scattering (at least in the spectral range of 300 – 630 nm).

Analysis of scattering indicatrices for sequential strippings of human skin epidermis has demonstrated that the g value averaged over five epidermal layers is $g = 0.89 \pm 0.02$ at $\lambda = 633$ nm. Treatment of the skin with psoralene (a cream used in phototherapy of psoriasis and other dermatoses) decreases g to 0.86 ± 0.01 [53, 94].

Apart from the traditional methods above for examining optics of scattering media (see for instance [42, 98, 107 – 110]), there are equally useful (even if less accurate) measuring techniques for biotissue optics which allow the rapid evaluation of optical parameters in real-time. We have already mentioned fast algorithms for the solution of the inverse problem [42, 59, 71, 80, 87, 88] and even simpler measuring schemes [71, 90]. One more example is tissue probing with an oblique laser beam. A simple analytical formula for the linear shift of the center of maximum diffuse reflection Δx has been suggested to facilitate the evaluation of the optical parameters of the medium [111]:

$$\Delta x = \frac{\sin \alpha_i}{\bar{n}(\mu_s' + 0.35\mu_a)} , \tag{10}$$

where α_i is the incidence angle of the beam, $\bar{n}$ is the mean refractive index of the scattering medium (the tissue is assumed to be in the air), and $\mu_s' \gg \mu_a$. It also follows from (10) that both the mean refractive index of a biotissue and the refractive indices of its scattering centers n_c and base matter n_0 should be measured independently since $\bar{n} = c_c n_c + c_0 n_0$ (c_c and c_0 are respective relative concentrations, $c_c + c_0 = 1$) and the $n_c/n_0 \equiv n$ ratio determines the scattering coefficient. For example, in a simple monodisperse model of scattering dielectric balls [104]

$$\mu_s' \cong 3.28\pi a^2 \rho \left(\frac{2\pi a}{\lambda}\right)^{0.37} (n-1)^{2.09} , \tag{11}$$

where a is the ball radius and ρ is the volume density of the balls. Formula (11) is valid for non-interacting Mie scatterers at $g > 0.9$, $5 < 2\pi a/\lambda < 50$, $1 < n < 1.1$.

It follows from (11) that even a 5% change in the refractive index of the base matter ($n_0 = 1.35 \rightarrow 1.42$), when that of the scattering centers is $n_C = 1.47$, will cause a 7-fold

decrease of μ_s'. In the limit of equal refractive indices, $n = 1$ $\mu_s' \to 0$.

Measuring refractive indices in biotissues and their constituent components is an important focus of interest in biotissue optics. Although these studies have rather a long history [34], the mean values of refractive indices for many tissues are lacking from the literature. According to [34], most of them have refractive indices for visible light in the 1.335–1.62 range (e.g. 1.55 in the horny skin layer, 1.62 in the enamel, and 1.386 at the lens surface). It is worthwhile to note that *in vitro* and *in vivo* measure may differ significantly. For example, the refractive index in rat mesenteric tissue *in vitro* was found to be 1.52 compared with only 1.38 *in vivo* [34]. This difference can be accounted for by the increased refractivity of base matter $\bar{n}$ due to impaired hydration. Indeed, optical properties of biotissues including refractive indices are known to depend on water content. The refractive indices of water over a broad wavelength range of 0.2–200 μm have been reported in [34]. Specifically, $n = 1.396$ for $\lambda = 0.2$ μm, $n = 1.335$ for $\lambda = 0.5$ μm, $n = 1.142$ for $\lambda = 2.8$ μm, and $n = 1.400$ for $\lambda = 3.5$ μm λ. The following relation was shown to be valid for the wavelength range corresponding to the best light transmission through biotissues [103] (λ in nanometers):

$$n_{H_2O} = 1.31848 + \frac{6.662}{\lambda - 129.2}\,.$$

Refractivity measurements in a number of strongly scattering biotissues at 633 nm performed with a fiber-optic refractometer have shown that fatty tissue has the largest refractive index (1.455) followed by kidneys (1.418), muscular tissue (1.410), then blood and spleen (1.400). The lowest refractive indices were found in lungs and liver (1.380 and 1.368 respectively) [112]. Also, it turned out that tissue homogenization does not significantly affect the refractive indices whereas coagulated tissues have higher refractive indices compared with native ones. Moreover, there is a tendency to decreasing refractive indices with increasing light wavelength from 390 to 700 nm characteristic of the majority of related abiotic materials. The spectral dependences of refractive indices for oxy and deoxyhemoglobins in the 450–820 nm wavelength range were obtained in [113]. An original method for measuring refractive indices of dentine matrix, taking advantage of its tubular structure and the ability to transmit light as in a waveguide, was proposed in [114]. n_0 for visible light in freshly-cut teeth was found to be 1.553 ± 0.001.

2.3 Controlling of optical properties of biotissues

Reflection, absorption, and scattering patterns in biotissues and blood can be effectively modulated by different methods [1–7, 10–14, 25, 33, 38–40, 94, 103, 114–137]. Staining (sensitization) of biological materials is extensively used to study mechanisms of interaction between their constituent components and light and also for diagnostic purposes and selective photodestruction of individual elements of living biotissues. This approach underlies the diagnosis and photodynamic therapy of malignant neoplasmas and UV-A photochemotherapy of psoriasis and other proliferative disorders [1–7, 10–14, 35, 38, 40, 78, 116].

It is possible to increase the transmission through soft tissues perfused with blood by their squeezing or stretching [117, 118, 122]. The optical enlightening of living tissue is due to its optical homogeneity achieved through the condensation of scattering centers (e.g. collagenous fibers in the muscular tissue) and the removal of blood and interstitial liquor (water) from the compressed site. This results in a higher refractive index of the base matter which becomes similar to that of collagenous fibers [see (11)]. Certainly, the absence of blood in the compressed area also contributes to altered tissue refractivity. The mechanisms underlying the effects of optical enlightening in biotissues were proposed in [116, 123]. It should be emphasized, however, that squeezing-induced effects in tissues containing little blood, such as sclera, are characterized by a marked inertia (a few minutes) because of the relatively slow water diffusion from the compressed region [103].

It is possible to achieve a marked impairment of scattering by matching the refractive indices of scattering centers and base matter by means of intratissue administration of appropriate agents. Conspicuous experimental optical enlightening in human sclera in the visible wavelength range induced by administration of verographin and trazograph solutions has been described in [124, 136]. Coordination between refractive indices in multicomponent biotissues showing polarization anisotropy (e.g. cornea) leads to its decrease [5, 6]. Concentration-dependent variations of scattering and transmission profiles in α-crystalline suspensions isolated from calf lenses are believed to be related to osmotic phenomena [133]. Osmotic and diffusive processes which occur in sclera treated with verographin and trazograph solutions are also important [136]. Osmotic phenomena appear to be involved when optical properties of biological materials (cells and tissues) are modulated by sugar, alcohol, and electrolyte solutions. This may interfere with the evaluation of hemoglobin saturation with oxygen or identification of such absorbers as cytochrome oxidase in biotissues by optical methods [130].

Natural physiological changes in cells and tissues are also responsible for their altered optical properties which may be used as a measure of these changes. For example, Ref. [134] presents a nearly parabolic dependence between the scattering coefficient and hematocrite values (H) in thin blood layers: $\mu_s \sim H(1 - H)(1.4 - H)$. The same paper reports optical characteristics of blood as a function of hemoglobin saturation with oxygen.

Experimental studies on optical enlightening changes in pathological skin and the management of reflectance and transmittance spectra using water, sunburn creams, and pharmaceutical products were carried out in [14, 126]. The observed effects appear to have been due to the introduction of additional scatterers or absorbers into the tissue or, conversely, to their washing-out. In addition, some of them were related to the immersion of refractive indices of scatterers and base matter.

UV irradiation causes erythema (skin reddening), stimulates melanin synthesis, and can induce edema and tissue proliferation if the radiation dose is sufficiently large [127, 128, 137]. All these photobiological effects may be responsible for variations in the optical properties of skin and need to be taken into consideration when prescribing phototherapy. Also, UV treatment is known to cause color development in the human lens [15].

Low temperatures (+12 °C) sometimes result in the so-called cold cataract, i.e. a sharp rise in the scattering coefficient due to protein aggregation [121, 135]. This process is reversed upon a rise of temperature.

Laser ablation or coagulation is usually accompanied by a change in the normal optical properties of the tissue [119, 120]. For example, ablation of aortal tissue using an eximer laser (308 nm) results in a 2.3–3.7-fold increase in its optical

density compared with the untreated material [119]. Coagulation of aortal tissue (100 °C, 300 s) does not significantly affect its absorption coefficient μ_a in the 350–1750 nm range (less than a 21.4% fall at 630 nm) whereas its reduced scattering coefficient μ_s' increases to 148.6% [120].

2.4 Short pulse propagation in biotissues

Based on the non-stationary radiation transfer theory, it is possible to analyse the time-dependent response of scattering tissues [138]. Such an analysis is important to provide a rationale for non-invasive optical diagnostic methods using time-resolved measurement of reflectance and transmittance in biotissues [1–3,139–155]. In the general form, the non-stationary RTT equation can be written in the form [138]

$$\frac{\partial}{\partial S} I(r,s,t) + t_2 \frac{\partial}{\partial t} I(r,s,t) = -\mu_t I(r,s,t) + \frac{\mu_s}{4\pi} \int_{4\pi} \left[\int_{-\infty}^{t} I(r,s',t') f(t,t')\, dt' \right] \times p(s,s')\, d\Omega' . \quad (12)$$

Compared with the stationary equation (2), the following notation is introduced into Eqn (12): t is time, $t_2 = 1/(\mu_t c)$ — is the average interval between interactions, and c is the velocity of light in the medium; $f(t,t')$ describes the temporal deformation of a δ-shaped pulse following its single scattering and can be represented in the form of an exponentially decaying function

$$f(t,t') = \frac{1}{t_1} \exp\left(-\frac{t-t'}{t_1}\right),$$

where t_1 may be a function of r and t_1 is the first moment of the distribution function $f(t,t')$ which describes the length of an individual scattering act at $t_1 \to 0, f(t,t') \to \delta(t-t')$. The radiative intensity $I(r,s,t)$ in Eqn (12) contains two components: the attenuated incident radiation and the scattering. This equation meets the boundary conditions (3) at $(r,s) \to (r,s,t)$.

When probing the plane-parallel layer of a scattering medium with an ultrashort laser pulse, the transmitted pulse consists of a ballistic (coherent) component, a group of photons having zigzag trajectories, and a highly intensive diffuse component [1–3]. Both unscattered photons and photons undergoing forward-directed scattering contribute to the intensity of the ballistic component (comprised by photons travelling straight along the laser beam). This component is subject to exponential attenuation with increasing sample thickness [see (1)]. This accounts for the limited utility of ballistic photons for practical diagnostic purposes in medicine.

The group of photons with zigzag trajectories includes photons which experienced only a few collisions each. They propagate along trajectories which only slightly deviate from the direction of the incident beam and form the first-arriving part of the diffuse component. These photons carry information about the optical properties of the random medium and parameters of any foreign object which they may happen to come across during their progress.

The diffuse component is very broad and intense since it contains the bulk of incident photons after they have participated in many scattering acts and therefore move in different directions and have different path-lengths. Moreover, the diffuse component carries information about the optical properties of the scattering medium, and its deformation may reflect the presence of local inhomogeneities in the medium. The resolution obtained by this method at a high light-gathering power is much lower than in the method measuring straight-passing photons. Two probing schemes are conceivable, one recording transmitted photons and the other taking advantage of their backscattering (see Fig. 6).

If, in the diffusion approximation (valid at $\mu_a \ll \mu_s'$), the tissue is homogeneous and semi-infinite, the size of both the source and the detector is small compared with the distance ρ between them at the tissue surface, and the pulse may be regarded as single, then the light distribution is described by the time-dependent diffusion equation [141, 142]:

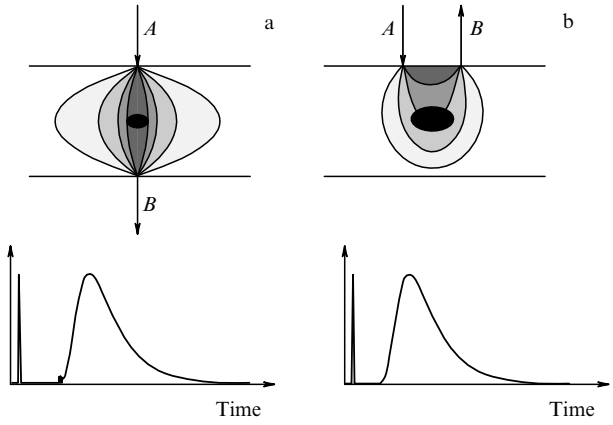

Figure 6. Typical schemes for time-resolved skin studies [139]: (a) recording transmitted photons, (b) backscattering regime, *A* — probing beam, *B* — detected radiation. The dark area in the centre of the scattering layer is a local inhomogeneity (tumor). Photon distributions in the medium are shown.

$$\left(\nabla^2 - c\mu_a D^{-1} - D^{-1} \frac{\partial}{\partial t}\right) U(r,t) = -Q(r,t), \quad (13)$$

which is in fact the generalization of the stationary equation (8). It is worth noting that the diffusion equation is equivalent to the equation for thermal conductivity [155]. The solution of Eqn (13) yields the following relation for the number of backscattered photons at the surface for unit time and from unit area $R(\rho,t)$ [141, 142]:

$$R(\rho,t) = \frac{z_0}{(4\pi D)^{3/2}} t^{-5/2} \exp\left(-\frac{\rho^2 + z_0^2}{2Dt}\right) \exp(-\mu_a c t), \quad (14)$$

where $z_0 = (\mu_s')^{-1}$

In practice, μ_a and μ_s' are estimated by comparing Eqn (14) with the shape of a pulse measured by the time-resolved photon counting technique. Experimentally measured optical parameters of many biotissues and model media obtained by the pulse method can be found in Refs [1–3,10–13,36, 37, 141–145]. An important advantage of the pulse method is its applicability to *in vivo* situations by virtue of μ_a and μ_s' separation during a single measurement in the backscattering regime. It seems appropriate to mention that a search for a more adequate approach to the description of biotissue response to laser pulses is underway (see for instance [146, 147]). Many publications are devoted to image transfer in biotissues and the evaluation of the resolving power of optical

tomographic schemes making use of the first-transmitted photons of ultrashort pulses [1 – 3, 139, 140, 148 – 152].

The use of ultrafast laser pulses gives rise to a local peak of intensity backscattered within a narrow solid angle owing to scattered light interference [153]. In the exact backward direction, the intensity of the scattered light is normally twice the diffuse intensity. The profile of the angular distribution of the so-called coherent peak depends on the transport mean path l_δ and the absorption coefficient μ_a. The angular width of the peak may be directly related to l_δ [153]: $\Delta\theta \approx \lambda/(2\pi l_\delta)$. In many hard and soft biotissues, such as human fat tissue, lung cancer tissue, normal and cataracted lens, myocardial, mammary, and dental tissues, the back-scattered coherent peak occurs when the probing laser pulse is shorter than 20 ps [153].

2.5 Diffuse photon-density waves

The frequency-domain method has recently been proposed for photon migration studies in scattering media. The method is designed to evaluate the dynamic response of scattered light intensity to modulation of the incident laser beam intensity in a wide frequency range from 0.1 to 10 GHz [1 – 3, 6, 115, 154 – 176]. The frequency-domain method measures the degree of modulation of scattered light intensity m_s and the corresponding phase shift relative to the incident light modulation phase $\Delta\Phi$. Compared with the time-dependent measurements described above, this method is more simple and reliable in terms of data interpretation and noise immunity, and can be realized with measuring devices used in optical communication and optical fiber dispersion studies [177]. The current measuring schemes are based on heterodyning optical and transformed signals [1 – 3, 6, 115, 154 – 176].

The development of the theory underlying this method resulted in the discovery of a new type of wave: photon-density waves or progressively decaying waves of enveloping photon density. Microscopically, individual photons make random migrations in a scattering medium, but collectively they form a photon-density wave at a modulation frequency ω that move away from a radiation source. Diffuse waves of this type are well known in other fields of physics (for example, thermal waves are excited upon absorption of modulated laser radiation in various media including biological ones [5, 178]). Photon-density waves possess typical wave-properties, e.g. they undergo refraction, diffraction, interference, dispersion and attenuation [1 – 3, 154, 158 – 161, 164 – 166].

In strongly scattering media with weak absorption far from the walls and a source or a receiver of radiation, the light distribution may be regarded as a decaying diffusion process described by the time-dependent diffusion equation for photon density (13). When a point light source with harmonic intensity modulation is used, placed at the point $r = 0$, $I(0, t) = I_0\left[1 + m_I \exp(j\omega t)\right]$.

The solution of Eqn (13) for a homogeneous infinite medium can be presented in the form [2]:

$$U(r, t) = U_{dc}(r) + U_{ac}(r, \omega)\exp(j\omega t)\,, \tag{15}$$

where

$$U_{dc} = \frac{I_0}{4\pi D r}\exp\left(-\frac{r}{l_d}\right),\quad U_{ac}(r,\omega) = \widetilde{U}_{ac}(r,\omega)\exp\left[-\mathrm{i}k_r(\omega)r\right],$$

$$\widetilde{U}_{ac}(r,\omega) = m_I\frac{I_0}{4\pi D r}\exp\left[-\mathrm{i}k_i(\omega)r\right],$$

$\omega = 2\pi\nu$ is the modulation frequency, $l_d = \mu_d^{-1}$ is the diffusive penetration depth, $k_r(\omega)$ and $k_i(\omega)$ are the real and imaginary parts of the photon-density wave vector respectively:

$$k = k_r - \mathrm{i}k_i = -\mathrm{i}\left(\frac{\mu_a c + \mathrm{i}\omega}{D}\right)^{1/2},$$

$$k_{r,i} = l_d^{-1}\left[\frac{(1+\omega^2\tau_a^2)^{1/2} \mp 1}{2}\right]^{1/2},\quad \tau_a^{-1} = \mu_a c\,.$$

A variable constituent of this solution is a going-away spherical wave with its center at the point $r = 0$ which oscillates at a modulation frequency ν and undergoes a phase shift relative to the phase value at point $r = 0$ equal to

$$\Delta\Phi = k_r(\omega)\, r\,. \tag{16}$$

Constant and time-dependent constituents of the photon density fall with distance, as $\exp(-r/l_d)$ and $\exp[-k_i(\omega)\, r]$ respectively. The length of a photon-density wave is defined by the relation

$$\Lambda_\Phi = \frac{2\pi}{k_r} = \frac{2\pi}{\omega}\left\{2cD\mu_a\left[1 + (1+\omega^2\tau_a^2)^{1/2}\right]\right\}^{1/2}, \tag{17}$$

and its phase velocity is

$$V_\Phi = \Lambda_\Phi \nu\,. \tag{18}$$

It follows that photon-density waves are capable of dispersion. Bearing in mind the possible medical implications of this finding (e.g. optical mammography), it is not difficult to calculate that for $\nu = 100$ MHz, $\mu_s' = 15$ cm^{-1}, $\mu_a = 0.0035$ cm^{-1}, and $c = (3\times 10^{10}/1.33)$ cm s^{-1}, the wavelength $\Lambda_\Phi = 13.4$ cm, and phase velocity $V_\Phi = 1.34\times 10^9$ cm s^{-1}.

For weakly absorbing media, when $\omega\tau_a \gg 1$,

$$\Lambda_\Phi^2 = \frac{8\pi^2 D}{\omega}\,,\quad V_\Phi^2 = 2D\omega\,,$$

$$m_U(r,\omega) \equiv \frac{\widetilde{U}_{ac}(r,\omega)}{U_{dc}(r)} = m_I\exp\left(r\sqrt{\frac{D}{c\mu_a}}\right)\exp\left[-r\left(\frac{\omega}{2D}\right)^{1/2}\right], \tag{19}$$

$$\Delta\Phi(r,\omega) = r\left(\frac{\omega}{2D}\right)^{1/2}.$$

Measuring $m_U(r,\omega)$, $\Delta\Phi(r,\omega)$ allows us to separately determine transport the scattering coefficient μ_s' and the absorption coefficient μ_a and evaluate the spatial distribution of these parameters.

Evidently, there is a close relationship between the two time-resolved methods for the assessment of optical properties of biotissues. In the case of pulse probing of a scattering medium, Fourier instrumental or computer-aided analysis of scattered pulses allows us to simultaneously obtain the amplitude-phase response of the medium for a continuous set of harmonics [1 – 3, 155, 162]. Figure 7 illustrates the typical behavior of the amplitude-phase response in a model scattering medium (whole or diluted milk) [2]. Such characteristics are useful for the spectroscopic examination of biotissues, e.g for *in vivo* evaluation of hemoglobin oxygenation [172] or blood glucose level [131].

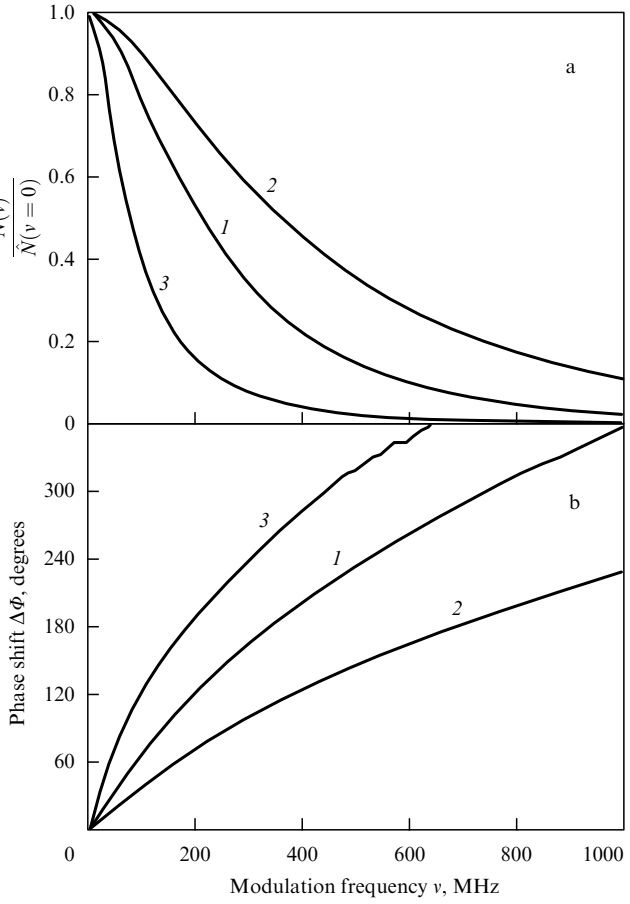

Figure 7. Amplitude (a) and phase (b) responses of the model medium (unskimmed (*1, 3*) and diluted (40%) (*2*) milk) obtained by the Fourier transformation of experimental pulse responses: *1, 2* — recording transmitted pulses, 2 cm thick cuvette, *3* — backscattering regime (large volume of unskimmed milk); the distance between irradiating and detecting optic fibers is $\rho = 2$ cm [2].

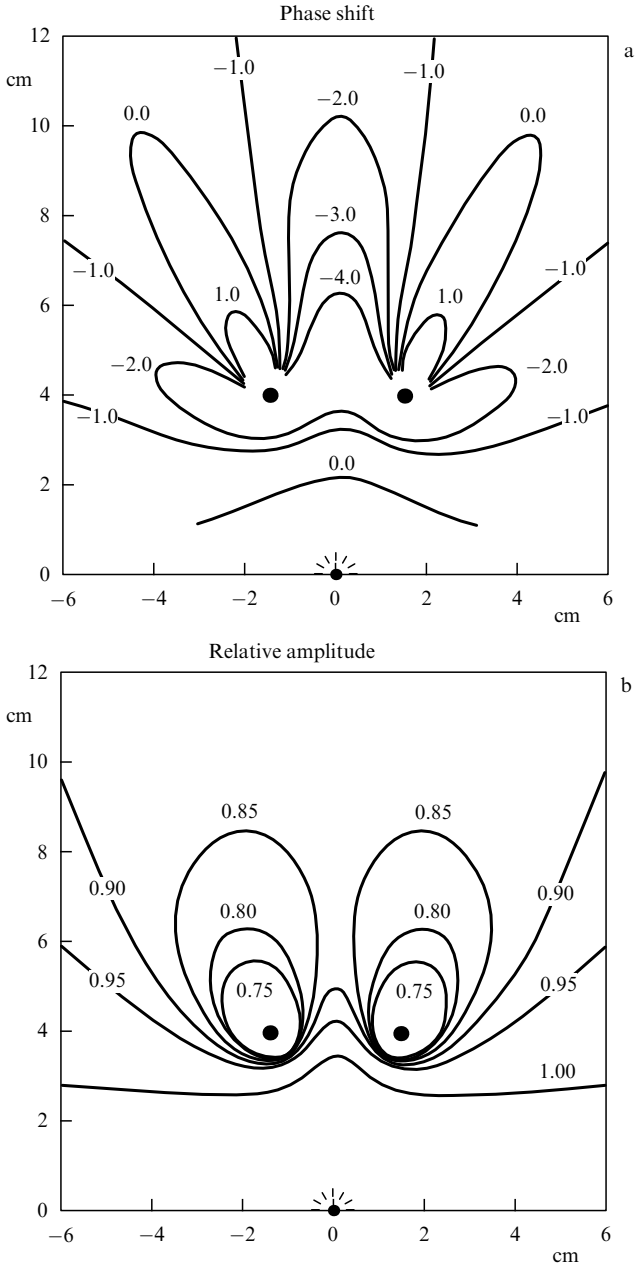

Figure 8. Theoretical distributions of the relative phase shift and intensity modulation at 200 MHz in an irradiated system of two absolute absorbers (balls 0.5 cm in diameter) placed in a homogeneous scattering medium ($\mu_s' = 10\ \text{cm}^{-1}$, $\mu_a = 0.02\ \text{cm}^{-1}$). The source is located at the origin and the absorbers at points (−2, 4) and (2, 4) [179].

Spatial resolution available using photon-density waves is crucial for the visualization of inhomogeneities. Theoretical considerations illustrated by Fig. 8 for two absorbing inhomogeneities in a scattering medium give evidence that their separate identification is feasible if the accuracy of the phase and wave amplitude measurements is not less than 1.0% and 2.0% respectively [179]. The predicted resolving power of diffuse tomography using photon-density waves is close to 1 mm, i.e. comparable with that of positron-emission and magneto-resonance tomography [154]. Important advantages of optical tomography are technical simplicity, the enhancement of an object's contrast by molecular stains, and the visualization of local metabolic processes.

Figure 9 presents images of tumor-containing female breast tissue outlined by contour lines for μ_a and μ_s' which were obtained by exposure to modulated visible and near IR radiation [2]. The tumor is readily discernible due to its high absorption and scattering coefficients.

In principle, a record-breaking resolving power of less than 1 mm can be achieved by taking advantage of interference of photon-density waves excited by spaced sources [164, 180].

Apart from the visualization of macroinhomogeneities in breast tissues, the method is useful in examining other tissue, e.g. brain and lungs. It also provides an insight into many physiological processes dependent on oxygen consumption by tissues and organs and related hemodynamic changes. One of the most important areas of application may be the evaluation of the oxygen distribution in a functioning brain [154]. Another example is the monitoring of neoplastic growth patterns including enhanced blood volume and blood deoxygenation, increased intracellular organelle content, and tissue calcification which may be important for the differentiation between benign and malignant tumors [154].

To conclude, it should be emphasized that high tissue density sometimes necessitates taking into consideration the length of an individual scattering act t_1 [see (12)] which may

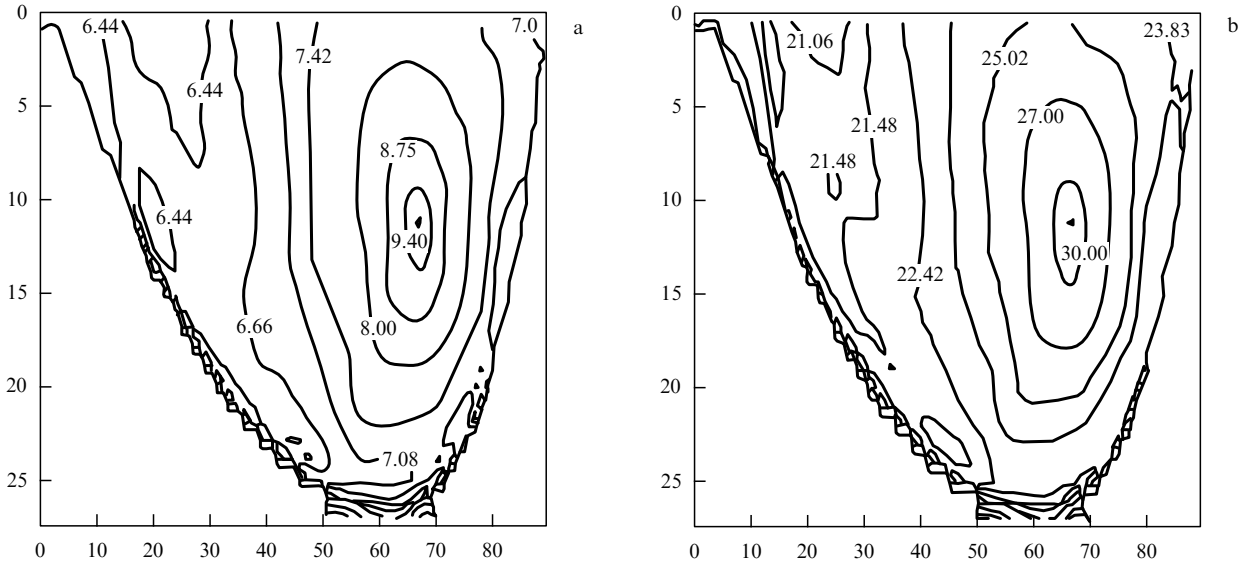

Figure 9. Reconstructed optical images of human cancerous breast tissue obtained by exposure to modulated radiation in the visible and near IR wavelength regions. Left: the image outlined by contour lines for the absorption coefficient μ_a (10^{-2} cm^{-1}); right: the same for the transport scattering coefficient μ_s' (cm^{-1}). The tumor is located near the point (70, 10); the coefficients have relative values [2].

prove comparable to the mean time-interval between interactions t_2 [175, 176]. Moreover, the widely used diffusion approximation imposes important constraints on the analysis of the optical properties of biotissues. Therefore, the development of more universal models of photon-density wave dispersion are well under way using new MC algorithms [176, 181, 182].

2.6 Propagation of polarized light in biotissues

Up to this point, we have ignored the vector nature of light travelling in scattering media, such as biotissues, because we assumed it to be rapidly depolarized during propagation in a randomly inhomogeneous medium. However, in certain tissues (e.g. eye tissues, cell monolayers, surface skin tissue, etc.), the polarization of transmitted or reflected light is easy to measure, using the degree of depolarization of the initially polarized light, the convertion of one polarization form to another, and the appearance of the polarized component in scattered light following object irradiation with unpolarized light as the most informative parameters characterizing the structure of biotissues and cell ensembles [3, 19, 21, 183 – 190). Published studies appear to have analysed polarization of multiply scattered light based on spatial photon diffusion with a practically isotropic angular radiation spectrum (see, for example, [41, 187, 191, 192]) or on small-angular scattering in large-scaled inhomogeneous media [21, 186, 187, 193, 194].

It should be emphasized, following [21], that the analysis of polarization in the case of small-angular multiple scattering is important for many problems pertaining to optical diagnosis of biomedia which can be represented as random systems with long-range correlations between fluctuations of dielectric permittivity [195] which display coherent scattering effects [153, 196] or may be expected to undergo fluctuations of polarized light similar to those in disordered media with large-scale inhomogeneities.

As regards practical implications, polarization techniques are believed to give rise to simplified schemes of optical tomography for therapeutic purposes compared with time and frequency (phase)-dependent methods and also provide additional information about the structure of biotissues [185, 197].

Let us first consider linearly polarized radiation in biotissues and model media. One of the first attempts to examine the depolarization of laser radiation in various biotissues is reported in [184]. The authors measured the components of radiation transmitted through a tissue layer and polarized parallel ($I_{||}$) and perpendicular ($I_{\perp}$) to the polarization plane of incident light. The measurements were taken in a narrow solid angle ($\approx 10^{-4}$ sr) in the incident light direction at 476, 488, and 514 nm using an Ar-laser or at 633 nm (He-Ne laser) and a beam diameter of about 1 mm. The radiation was considered depolarized when $I_{||}/I_{\perp} = 2$. This ratio varied from 300 to 1, depending on the tissue type and thickness. The light path l_p at which the radiation underwent depolarization ($I_{||}/I_{\perp} = 2$) was a tissue parameter. It turned out that l_p values for white substance and cortical brain tissue were significantly different (0.19 and 1.0 mm at 476 – 514 nm and 0.23 and 1.3 mm at 633 nm respectively). Human skin dermis (devoid of blood) had the depolarization length of $l_p = 0.43$ mm at 476 – 514 nm and 0.46 mm at 633 nm. The depolarization length decreased in the pathologically altered aortal wall to 0.39 mm during calcification and 0.33 mm at the necrotic ulceration stage compared with $l_p = 0.54$ mm ($\lambda = 476 – 514$ nm) in the normal tissue. Whole blood at a low hematocrit value had a long depolarization length of 4.0 mm at 633 nm.

Clearly, the depolarization length must be close to the photon transport mean path l_δ since it defines the distance over which the scattered light direction becomes wholly random and is responsible for the randomness of the polarization plane of linearly polarized light [183, 185]. Since l_δ determines the reduced scattering coefficient $\mu_s' = \mu_s(1 - g)$, l_p must show strong dependence on the parameter of scattering anisotropy. The above experimental results [184] confirm this observation. Specifically, blood has the largest g value compared with other biotissues ($g \approx 0.982 – 0.995$) [198].

It is worthwhile to note that contrary to depolarization, attenuation of collimated light is defined by the total attenuation coefficient [see (1)] which is significantly higher than μ_t for many tissues. Therefore, situations are conceivable in which the initial polarization of the forward scattered light is still apparent in the absence of unscattered light. The existence of different regimes with persisting or disturbed linear polarization depends on the particle size and content in the host biotissue [183].

A study [185] confirmed experimentally that linear polarization is preserved over 2.5 transport paths $l_\delta\big(P = (I_{\|} - I_\perp)/(I_{\|} + I_\perp) = 0.1\big)$. For example, $l_\delta \approx 0.48$ mm for the skin which has $\mu_a \approx 0.4$ cm^{-1} and $\mu_s' \approx 20$ cm^{-1} in the red and near IR wavelength ranges respectively. Therefore, light can travel a distance of 1.2 mm in the skin without the complete loss of linear polarization. This path in a biotissue corresponds to a delay time of about 5.3 ps allowing polarization images of tissue macroinhomogeneities to be obtained which are equivalent to inhomogeneities revealed by photon selection techniques described in previous sections. An important advantage of polarization visualization, in addition to the selection of diffusely scattered photons, is the possibility to exclude specular reflection from the tissue surface [199] (for example, by varying the angle of irradiation and detecting reflected light [185]). This provides a novel opportunity to record birefringence and optical activity of surface layers (e.g. in the skin), besides macroinhomogeneities detectable by time-dependent methods. Ref. [199] demonstrates an experimental visualization of facial skin microvessels using the polarization contrast technique.

Information about the optical parameters of a scattering medium can be obtained not only from the degree of depolarization of the previously polarized radiation but also from the degree of polarization of the initially non-polarized light beam propagating in a scattering medium. In media containing large-scale scatterers (a common biotissue model), depolarization is a higher order effect compared with polarization ($\sim \theta^2$) [21].

In weakly absorbing media showing small-angular multiple scattering, the degree of linear polarization for a Henyey–Greenstein-like function [see (6)] is described by the following formula [21]:

$$P = -\frac{(\mu_s' z)^4}{2\theta^2}\left[\sqrt{1+\left(\frac{\theta}{\mu_s' z}\right)^2} - 1\right]^2\left[1+\left(\frac{\theta}{\mu_s' z}\right)^2\right]. \quad (20)$$

This means that, in a very small angle range $\theta \ll \mu_s' z$, the degree of polarization does not depend on the depth

$$P = -\frac{\theta^2}{8}, \quad (21)$$

at the wings of the scattering indicatrix ($\theta \gg \mu_s' z$), it tends to

$$P = -\frac{\theta^2}{2}, \quad (22)$$

which equals the degree of polarization of singly scattered light.

Let us now consider the transformation of any polarization type (linear, circular or elliptical) in a scattering medium with typical biotissue parameters and compare the penetration depth of circular and linear polarization in different media. To this end, let us examine a monochromatic plane wave incident onto an isolated scatterer [191, 200–202]. The polarization state of scattered light is described by the Stokes vector

$$\mathbf{I}_S = M \cdot \mathbf{I}_i, \quad (23)$$

where M — 4×4 is the scattering matrix (or Mueller's matrix) and $\mathbf{I}_i$ is the Stokes vector of incident light defined through

$$\mathbf{I} = \begin{bmatrix} I \\ Q \\ U \\ V \end{bmatrix}, \quad (24)$$

where $I, Q = \langle E_x E_x^* \pm E_y E_y^* \rangle$; $U, V = \langle E_x E_y^* \pm E_y E_x^* \rangle$; E_x and E_y are the orthogonal components of the electric field vector and braces $\langle\ \rangle$ indicate averaging over time.

In the general case, light scattered at a particle becomes elliptically polarized. For spherically symmetric particles of an optically inert material,

$$M = \begin{vmatrix} M_{11} & M_{12} & 0 & 0 \\ M_{12} & M_{11} & 0 & 0 \\ 0 & 0 & M_{33} & M_{34} \\ 0 & 0 & -M_{34} & M_{33} \end{vmatrix} \quad (25)$$

elements of the light scattering matrix (LSM) depend on the scattering angle θ, the wavelength, and geometrical and optical parameters of the scatterers. The degree of linear polarization of scattered light is defined through the Stokes parameters as

$$P_L = \frac{Q_S}{\mathbf{I}_S}, \quad (26)$$

and that of circular polarization as

$$P_C = \frac{M_{33}}{M_{11}}. \quad (27)$$

For an ensemble of interacting particles in the single scattering approximation [5, 6], LSM elements have the form

$$M_{ij}(\theta) = M_{ij}^0(\theta)\, NF(\theta), \quad (28)$$

where M_{ij}^0 are the LSM elements of an isolated particle, N is the number of scatterers, and $F(\theta)$ is the interference term taking into account the spatial correlation of particles. Note that the LSM elements (M_{ij}/M_{11}) do not depend on whether account is taken of spatial correlation of scatterers and coincide with LSM elements for isolated particles (in a monodisperse system). Given the known character of the Stokes vector transformation for each scattering act, the state of polarization following multiple light scattering in a dimensional medium can be found using various approximations of the multiple scattering theory [186, 187] or the MC method [19, 186]. For small particles, the effects of multiple scattering are apparent as the broken symmetry relationship between LSM elements [see (25)], $M_{12}(\theta) \neq M_{21}(\theta)$, $M_{33}(\theta) \neq M_{44}(\theta)$, and a significant reduction of linear polarization of the light scattered at angles close to $\pi/2$ [187].

For a system of small spatially uncorrelated particles, the degree of linear ($i = L$) and circular ($i = C$) polarization in the far region of the initially polarized (linearly or circularly) light transmitted through a layer of width d is defined by the relation [186]

$$P_i \cong \frac{2d}{l_s}\sinh\left(\frac{l_s}{\xi_i}\right)\exp\left(-\frac{d}{\xi_i}\right), \quad (29)$$

where $l_s = 1/\mu_s$,

$$\xi_i = \left(\frac{\zeta_i l_s}{3}\right)^{1/2} \tag{30}$$

is the characteristic depolarization length for a layer of scatterers, $d \gg \xi_i$, $\zeta_L = l_s/[\ln(10/7)]$, $\zeta_C = l_s/(\ln 2)$. Hence, the characteristic depolarization length for the incident light with linear polarization is $\sqrt{2}$ times that for scattered light retaining circular polarization. Relations (29) and (30) are equally valid for a system of large spherical particles (of wavelength-size, Mie scattering) if l_s is substituted by the transport path $l_\delta \equiv 1/\mu_s'$.

Results of numerical analysis by the MC method and of model experiments using aqueous latex suspensions with different particle sizes [186] suggest three regions for the linear to circular polarization ratio in transmitted light $R \equiv P_L/P_C$, depending on d/l_δ (see Fig. 10). R increases in the Rayleigh region in accordance with expression (29), remains unaltered in the intermediate region, and decreases in the Mie R scattering region. Such behavior is associated with the transition from isotropic single scattering to anisotropic. The qualitative physical explanation of different depolarization patterns is that the presence of strong backscattering has no adverse effect on linear polarization; at the same time, strong backscattering in the case of circular polarization is equivalent to the inversion of polarization patterns (as mirror reflection), i.e. depolarization. Therefore, for a pencil like single-scattering indicatrix (anisotropic scattering), the degree of circular polarization of light travelling in a layer must persist longer than the degree of linear polarization.

To summarize, biotissues differing in terms of pathological conditions or functional activities must respond differently to probing with linearly and circularly polarized light. This phenomenon can be used in optical tomography for medical purposes and for the evaluation of optical and spectroscopic parameters of biotissues.

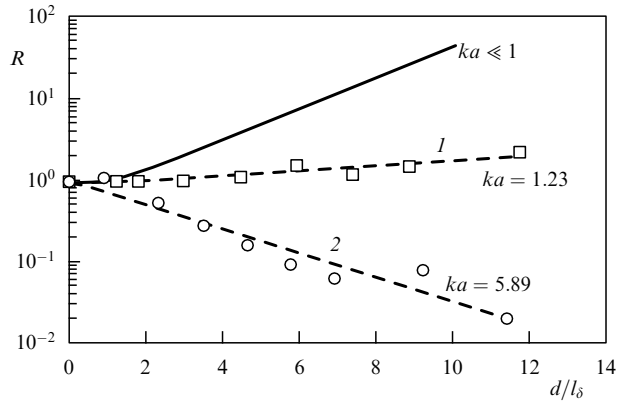

Figure 10. Semilogarithmic dependences of the degree of polarization ratio $R \equiv P_L/P_C$ on d/l_δ for three ka values, ka, $k = 2\pi/\lambda$. The solid line corresponds to Rayleigh scattering ($ka \ll 1$) and the dotted lines indicate a correspondence between experimental findings and Eqn (29) at $l_s = l_\delta$. The experimental points are measurements for aqueous suspensions of polystirol latex spherical particles having diameter 0.22 (*1*) and 1.05 (*2*) μm, $\lambda_0 = 670$ nm [186].

3. Optical properties of transparent biotissues

3.1 Optical models of eye tissues

Healthy tissues of the anterior eye chamber, e.g. the cornea and lens, are highly transparent for visible light due to their ordered structure and the absence of strongly absorbing chromophors. Scattering is an important feature of light propagation in eye tissues. The size of the scatterers and the distance between them are smaller than or comparable with the wavelength of visible light and the relative refractive index of the scattering matter is equally small ('soft particles'). Typical eye tissue models are long round dielectric cylinders (corneal and scleral collagenous fibers) or spherical particles (lens protein structures) having refractive index n_C and chaotically (sclera, opaque lens) or orderly (transparent cornea and lens) distributed in the isotropic base matter with refractive index $n_I \leqslant n_C$ [3, 5, 8, 16, 17, 124, 203, 205]. Light scattering analysis in eye tissues is possible using a single scattering model owing to the small scattering cross-section (soft particles).

In case of disordered scatterers, the resultant field intensity is the total intensity of fields scattered by individual particles. For ordered scatterers, fields, rather than intensities, should be summed to take into account effects of interference arising in the presence of the near order of scatterers. In the integral form, the scattering indicatrix for symmetric scattering of particles with pair correlation is described by the expression [3, 5, 8, 16, 17, 204, 205]:

$$I(\theta) = I_0(\theta)\left\{1 + \rho\int_0^\infty \left[g(r) - 1\right]\exp\left[\mathrm{i}(\mathbf{S}_1 - \mathbf{S}_0)\,\mathbf{r}\right]\mathrm{d}^3 r\right\} = I_0(\theta)\,F, \tag{31}$$

where $I_0(\theta)$ is the indicatrix of an isolated particle, θ is the scattering angle, ρ is the particle density, $g(r)$ is the distribution function of scattering centers (local to average density ratio for scattering centers (see also Fig. 11), for non-interacting centers $g(r) \to 1$), $\mathbf{S}_0$, $\mathbf{S}_1$ are unit vectors for incident and scattered waves, $\mathbf{r}$ is the radius-vector and $\mathrm{d}^3 r$ is the volume of a scatterer, and F takes into account the effects of interference.

Relation (31) is valid for a monodisperse system of scatterers and can be used provided a scattering indicatrix

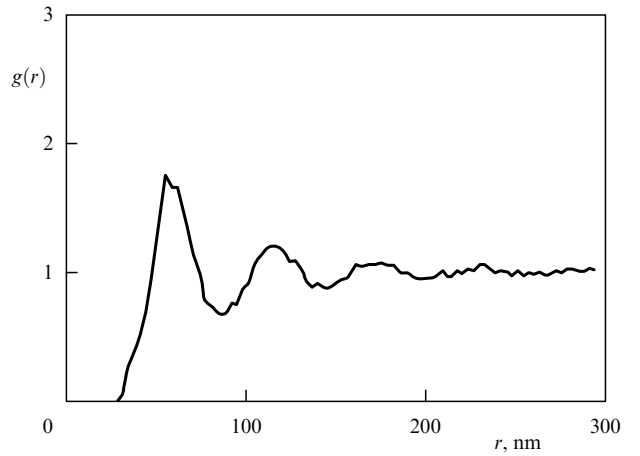

Figure 11. The distribution function of scattering centres in the corneal stroma of rabbit eye deduced from the analysis of electron micrographs of tissue sections [204, 205].

for a single particle $I_0(\theta)$ is available from computations based on the Mie theory and corresponding approximate relations. Polydispersion for randomly distributed scatterers (e.g. in a sclera model) is easy to take into consideration using gamma-distribution of particles by their radii [124].

It is much more difficult to take into account polydispersion in ordered biotissues such as transparent cornea or lens. In the simplest case of a two-phase system of scatterers, an expression analogous to (31) can be found using four structural functions $g_{11}(r)$, $g_{22}(r)$, $g_{12}(r)$ and $g_{21}(r)$ which characterize the interaction between particles of similar and different types [206]. A two-phase system made up of an ensemble of equally-sized small particles and a minor fraction of large ones provides a good model of pathological tissue, e.g. a cataracted lens.

For a long-cylinder system, the interference term F is defined by the expression [8, 204, 205]:

$$F = 1 + \rho \int_0^\infty J_0(\mathbf{S} \cdot \mathbf{r}) \cdot r\big[g(r) - 1\big]\, \mathrm{d}r\,, \tag{32}$$

similarly, for an ensemble of spherical particles [5, 16, 17]

$$F = 1 + 4\pi\rho \int_0^\infty r^2 \big[g(r) - 1\big] \left[\frac{\sin(\mathbf{S} \cdot \mathbf{r})}{(\mathbf{S} \cdot \mathbf{r})}\right] \mathrm{d}r\,, \tag{33}$$

where J_0 is the zero order Bessel function, $|\mathbf{S}| = 2k \sin(\theta/2)$, $k = 2\pi n/\lambda_0$.

The intensity of collimated light transmitting through a scattering tissue layer with a mean scatterer density ρ and thickness l is defined by the expression

$$I = I_0 \exp(-\rho\sigma_s l)\,, \tag{34}$$

where I_0 is the incident beam intensity, and the scattering cross-section is

$$\sigma_s = \frac{1}{\rho I_0} \int_{4\pi} I(\theta)\, \mathrm{d}\Omega\,. \tag{35}$$

3.2 Transmission and scattering spectra of eye tissues

Corneal transmittance was calculated using a model monodisperse system of long dielectric non-absorbing cylinders (fibrils) of 26 nm in diameter and refractive index $n_C = 1.470$. The cylinders were orderly oriented parallel to the corneal surface in the base matter ($n_I = 1.345$). Figure 12 demonstrates the transmittance anisotropy for linearly polarized radiation and the marked effect of scattering on corneal transmittance in the UV spectral region.

The lens is less transparent than the cornea. The visible light passing through the human lens undergoes an appreciable degree of both scattering and absorption by different chromophors including protein-bound tryptophane, kynurenin (3-HKG), and age-related protein (responsible for lens yellowing in aged subjects) [15]. The 3-HKG content slightly decreases with age. In the single-scattering model being examined, absorption is taken into account by introducing a complex refractive index for the scatterers [207]:

$$n(\lambda) = n' + \mathrm{i}n'' = n' + \mathrm{i}\big[tn_t''(\lambda) + kn_k''(\lambda) + pn_p''(\lambda)\big]\,, \tag{36}$$

where the coefficients t, k, and p characterize the contribution of each chromophor to absorption. Age-related changes in the lens optical properties are as a rule due to the appearance of scatterers having increased diameters and refractive index and also to the enhanced content of age-related protein [15, 125]. Figure 13 presents collimated transmittance spectra

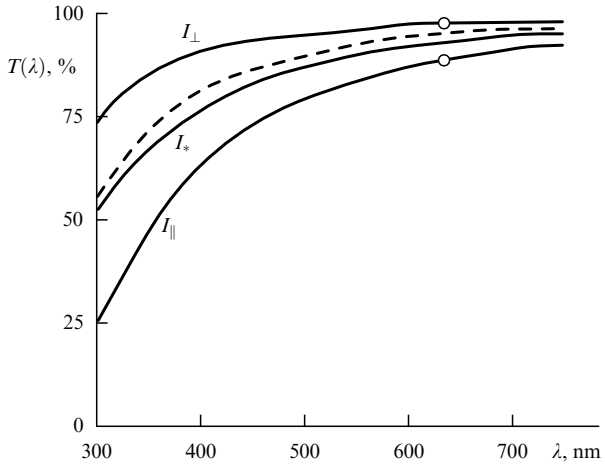

Figure 12. Collimated transmittance spectra of the human cornea: $I_\parallel$, $I_\perp$ and I_* are calculated spectra for two orthogonal linear polarizations and unpolarized light, $I_\parallel$ — light polarization parallel to fibrils (calculations were made for the light normally incident on the corneal surface; they are valid for the peripheral corneal portion where the fibrils are similarly oriented in tissue layers). The cornea is 0.46 mm thick, with a scatterer density $\rho = 3 \times 10^{10}$ cm^{-2}. The dotted line shows the experimental data for unpolarized light. Circles are measurements for two orthogonal polarizations at $\lambda = 633$ nm [16].

calculated using 'young' and 'old' lens models. A remarkable difference between the shortwave portions of the two profiles is readily apparent. Experimentally obtained transmittance spectra for senile and cataracted lenses are shown in Fig. 14 [207]. Age-related variations in the composition of scatterers and absorbers lead to significant differences in scattering spectra. There is a qualitative correlation between the experimental findings and the calculated values for both backscattering and scattering at 90° (see, for instance, Fig. 15) [207, 208].

Figures 16 and 17 demonstrate the possibility of making an opaque tissue (sclera) more transparent and transferring from a multiple-scattering mode to a single-scattering one by means of substituting the base matter by a substance with a higher refractive index [209]. The results of MC simulation agree fairly well with experimental data [124, 209]. The refractive indices of fibrils and base matter in a 1 mm thick opaque sclera are $n_C = 1.470$ and $n_I = 1.345$ respectively. The model of sclera examined in this study was a monodisperse system of dielectric cylinders (fibrils) with an average diameter 100 nm randomly oriented parallel to the sclera plane.

3.3 Polarization properties of eye tissues and other transparent biological objects

It has already been shown that light propagation in opaque multiply scattering biotissues depends not only on the scattering and absorption coefficients and the scattering phase function but also on the polarization properties of the tissue. The latter in turn depend on the scatterers' size, morphology, refractive index, internal structure, and optical activity of material [5, 98, 107, 108, 191, 200–202]. The polarization properties of elastically scattered light are described by a 16-element scattering matrix (SM), each element being dependent on the wavelength, size, shape, and material of the scatterers [see (23)–(25)].

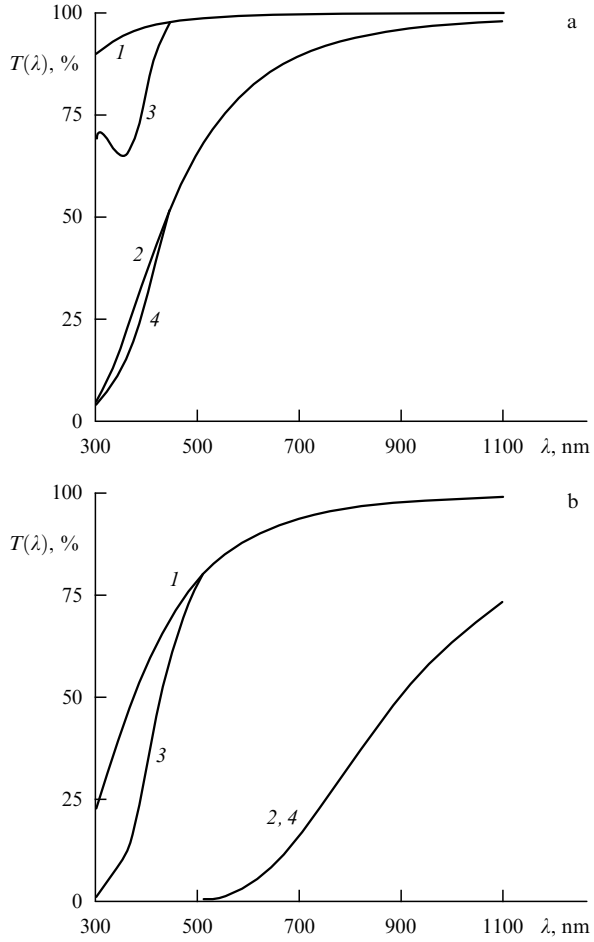

Figure 13. Collimated transmittance spectra of the human lens calculated for ordered (*1*, *3*) and disordered (*2*, *4*) scatterers. *1*, *2* — in the absence of absorption, *3*, *4* — with absorption; young lens model (diameter of scatterers $d = 0.02$ μm, $n' = 1.43$, $t = 0.003$, $k = 0.005$, $p = 0$) (a); old lens model ($d = 0.04$ μm, $n' = 1.47$, $t = 0.003$, $k = 0.002$, $p = 0.015$) (b). Volume density of scatterers $w = 0.3$, $n_I = 1.345$, lens thickness 5 mm [27].

Measurements of the Mueller matrix elements of transparent biological tissues and fluids are feasible with the help of laser polarizing nephelometers (LPN) widely used to examine bioobjects [3, 5, 6, 17, 18, 187, 190, 201, 210, 211].

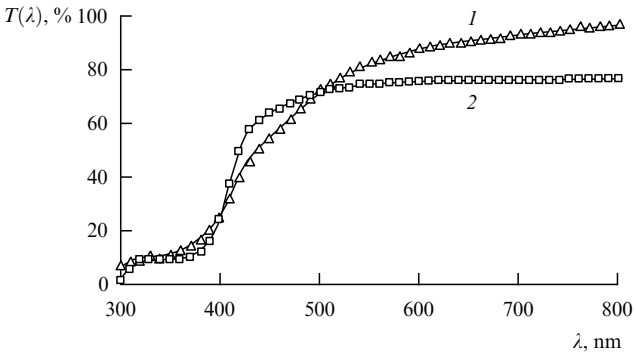

Figure 14. Experimental total transmittance spectra of isolated human lens: *1* — normal lens of a 56 year-old subject, *2* — cataracted lens (88 years). Measurements were made on a spectrophotometer with an integrating sphere [207].

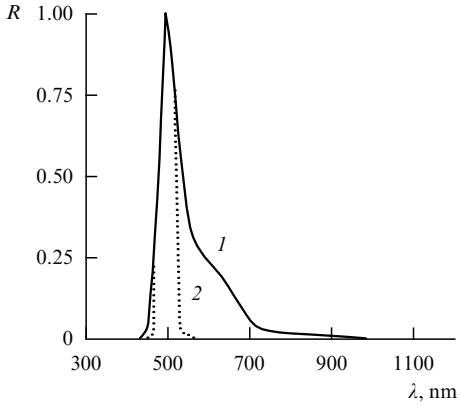

Figure 15. Calculated and experimental scattering spectra of the lens at 90° (relative units, from [208]). Calculations were made for a mixture of ordered small particles (99%:1%) having diameter $d = 0.06$ μm ($t = 0.003$, $k = p = 0.03$, $n_0 = 1.345$, $n_1 = 1.47$) and large disordered particles ($d = 0.6$ μm, $t = 0.003$, $k = 0$, $p = 0.1$).

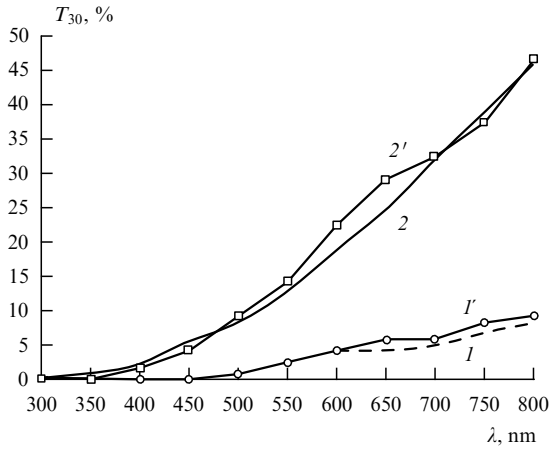

Figure 16. Transmittance spectra of human sclera calculated by the MC method (*1*, *2*) and experimental (*1′*, *2′*) (taking into account forward-directed scattering 30°) as functions of the duration of exposition to a clearing agent trazograph (60%): $1' - t = 0$; $2' - t = 50$ min and the variation in the refractive index of the base matter *1* — $n_I = 1.345$, *2* — 1.395, $n_C = 1.474$ [209].

The principle of LPN operation is the modulation of the polarization of a primary laser beam followed by scattered light demodulation (transformation of polarization modulation to intensity modulation) using phase ($\lambda/4$) plates rotating at a certain speed in the incident and scattered beams.

The measurement of angular dependencies of SM elements in a human lens shows their significant difference for clear and opaque (cataracted) eyes (Fig. 18). This difference may be due to the appearance of large non-spherical scattering particles in the turbid lens medium (due to aggregation of high molecular-weight proteins).

The comparison of transmittance spectra (see Figs 13 and 14) and angular dependencies of SM elements measured at the same wavelength indicates that the latter are more sensitive to variations in the structure of scattering media. This allows measurement of SM elements to be used for early diagnosis of structural changes in a biotissue, e.g. those caused by a developing cataract.

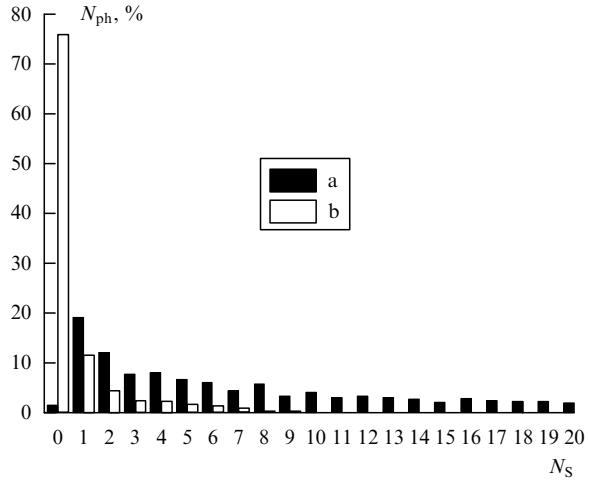

Figure 17. Distribution histograms for the number of scattering events N_S experienced by photons passing through the sclera N_{ph} (% of the total), (a) normal sclera model, $n_I = 1.345$, (b) partially cleared sclera model, $n_I = 1.410$, $n_C = 1.474$, $\lambda = 633$ nm [209].

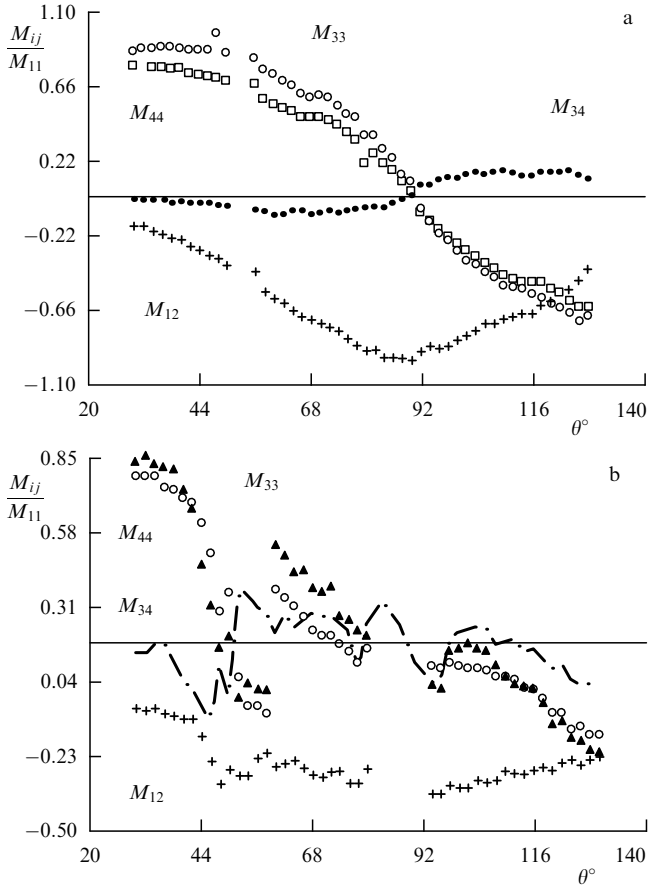

Figure 18. Experimental angular dependences for SM elements of a normal lens 5 hours after the death of a 56 year-old subject (a) and a cataracted lens 5 hours after the death of an 88 year-old subject (b) [207].

This inference can be illustrated by the results of direct model experiments presented in Fig. 19 [6, 115, 212]. The measurements were performed in an α-crystalline solutions (quasimonodisperse particle fraction about 0.02 μm in diameter) from a freshly isolated calf lens (a contribution by J Clauwaert, University of Antwerp, who also participated in the experiment) and in solutions of high molecular-weight proteins (mean diameter 0.8 μm) from opaque lenses [212]. The figure shows that measurements of the indicatrices of SM elements permits the identification of a coarsely dispersed fraction of scatterers which is difficult to achieve by spectrophotometry because the decrease in sample transmittance does not exceed 1%.

Laser polarization nephelometry may be employed for *in vitro* examination of various eye tissues, from cornea to retina. *In vivo* measurements in the intact eye are equally feasible provided fast LPN is used to exclude a sensory-motor eyeball response. In this case, structural information about selected eye tissues can be obtained to diagnose cataract and other ophthalmological disorders.

A survey of rabbit eye SM has demonstrated that the aqueous humor in the anterior eye chamber is actually a transparent isotropic substance exhibiting weak light scattering properties (the intensity of scattered light does not exceed 1.5–2% of the incident light intensity) due to the presence of dissolved organic components [213, 214]. Results of an SM study in the vitreous body indicate that its amorphous tissue does not affect the polarization of straight transmitting light offering the possibility to examine the ocular fundus and visualize the optic nerve structure which is important for early diagnosis of glaucoma [215]. On the other hand, certain pathological changes in the vitreous body may be responsible for the alteration of SM elements. Specifically, a minor intraocular hemorrhage is easy to identify by virtue of conspicuous light scattering from erythrocytes [213, 214].

The angular dependence of SM elements in a monolayer of disk-shaped or spheroidal erythrocytes in relation to their packing density was examined in Ref. [18]. The angular dependence of M_{11} in both cell types turned out to be influenced by the packing density in the angular scattering range of $\theta = 15^\circ - 16^\circ$. Angular dependences of M_{11}, M_{22}, M_{33}, and M_{21} at $\theta = 110^\circ - 170^\circ$ were found to be far more affected by the shape of the scatterers than by their concentration. It was possible to derive the refractive indices of erythrocytes from measurements of the M_{12} size at scattering angles $\theta \approx 140^\circ - 160^\circ$. A study [190] revealed the high susceptibility of the angular dependences of SM elements (M_{11} and M_{12}) to the degree of erythrocyte aggregation in blood plasma.

SM measurements were also used to examine the formation of liposome complexes with plague capsular antigen [216] and various particle suspensions, e.g. those of spermatozoid spiral heads and different bacterial species [201, 203]. The angular dependences of the normalized element M_{34} for different bacteria turned out to be oscillating functions (similar to those in Fig. 19) whose maxima positions are very sensitive to the varying size of bacteria. This allows bacterial growth to be followed up [217, 219]. Determination of SM elements is equally promising for more effective differentiation between blood cells by time-of-flight cytometry [202, 220].

4. Conclusion

The present review deals only with few a aspects of light-biotissue interactions, being focused on light scattering by random and quasi-ordered structures. Results of numerous

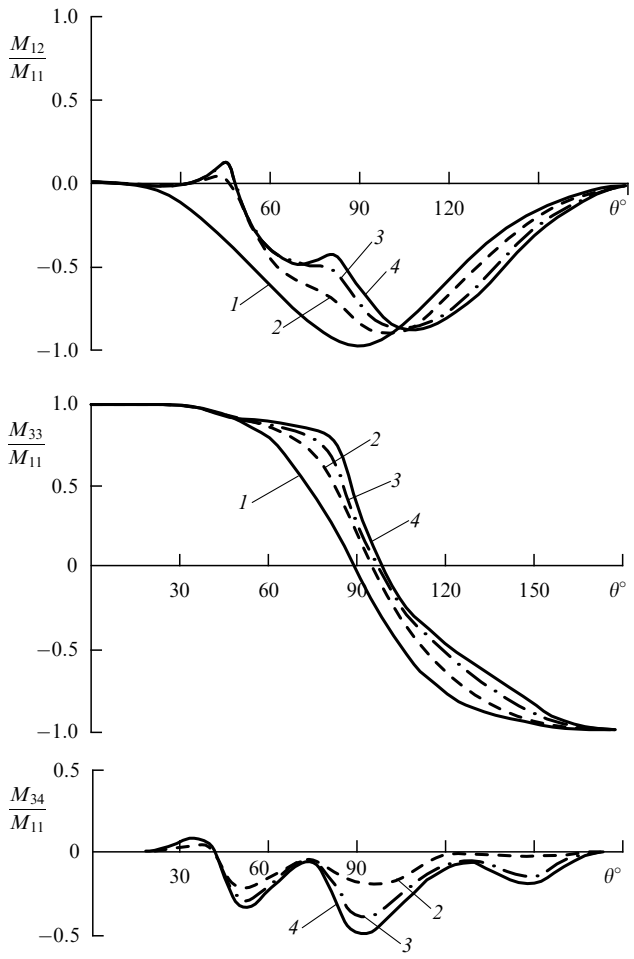

Figure 19. Indicatrices for SM elements of α-crystallin solutions and a fraction of large-size scatterers isolated from the cataracted lens. The relative volume concentrations of α-crystallin $w_1 = 0.3$ and the large-particle fraction w_2: *1* — $w_2 = 0$ ($\tau = 99\%$); *2* — $w_2 = 5 \times 10^{-5}$ ($\tau = 98\%$); *3* — $w_2 = 1.4 \times 10^{-4}$ ($\tau = 94\%$); *4* — $w_2 = 2.5 \times 10^{-4}$ ($\tau = 90\%$), τ is the transmittance of the 5 mm thick solution at $\lambda = 633$ nm.

studies on scattering events emphasize the necessity of an in-depth evaluation of the optical properties of biotissues with different structural organization. At present, light propagation in biotissues is fairly well described in qualitative (and sometimes in quantitative) terms which provides a sound basis for the implementation of different diagnostic, therapeutic, and surgical modalities. At the same time, the estimation of optimal irradiation doses or the choice of right diagnostic clues sometimes encounter great difficulty for the lack of reliable criteria for the optical parameters of biotissues.

Traditional spectrophotometry or angular and polarization measurements are useful to characterize biotissues but need to be improved if more sophisticated tissue models are to be obtained and applied to biomedical studies. Such models must take into consideration the spatial distribution of scatterers and absorbers, their polydisperse nature, optical activity, and the birefringence properties of the materials of which scatterers and base matter consist.

It is also necessary to further develop methods for the solution of inverse scattering problems with due regard for the real geometry of the object and the laser beam, which might be equally valid for the arbitrary ratio of scattering and absorption coefficients to the scattering anisotropy factor. The inverse MC method [53, 59, 91] is sometimes useful, but the fast computation required for practical medical diagnostics and dosimetry should be based on approximate solutions of the radiative transport equations.

Extensive studies are underway to better understand the role of photon-density waves and their use in phase modulation methods to obtain optical characteristics of biotissues [1 – 3, 154]. They are expected to bring about novel algorithms for the reconstruction of three-dimensional tissue images and practical applications of diffuse optical tomography.

The scattering matrix technique has long been used in optics and is currently applied by many authors to investigate the properties of biotissues and cell suspensions. The intensity matrix (Mueller matrix) is normally employed for the purpose, but the use of double-frequency lasers (e.g. a Zeeman laser) allows amplitude matrix elements to be measured thus offering the possibility to simplify the inverse problem solution for many biological structures [201].

Radiation dosimetry is an important line of research in laser biophysics. The basic principles of laser dosimetry are well-known, but further development of three-dimensional models should be encouraged to be able to consider specific features of biotissues and cell ensembles, the technology of photoeffects, and the optical characteristics of radiation sources.

Biotissue optics being a vast area of research, this review does not touch upon coherent techniques which measure diffraction and interference and take advantage of confocal and holographic microscopy. They need to be considered in a separate paper. Relevant data can be found in [1 – 5, 6, 23 – 30, 33, 135, 136, 221 – 229]. Also of interest for inhomogeneous tissue optics are speckle-optic methods and speckle-interferometry [230, 231]. Useful information about coherent techniques and their applications to cell and tissue optics can be found in a few excellent reviews [196, 232]. Ref. [232] is concerned with physical mechanisms of cell movements and laser Doppler anemometry as a principal method for non-invasive monitoring of cell motion and their contents, which are very promising for further *in vivo* biotissue studies.

The polarization properties of biotissues to which the present review is largely devoted are of primary importance for physiological polarization optics, the fundamentals of which are reviewed in Ref. [233].

Acknowledgments. I wish to thank Yu M Romanovskiĭ for suggesting the idea of writing this review and A V Priezzhev for valuable comments. The collaboration of S R Utz, I L Maksimova, D A Zimnyakov, I V Yaroslavskiĭ, I L Kon, and D M Zhestkov is acknowledged. I am especially grateful to S P Chernova for her help in the preparation of the manuscript.

References

1. Müller G et al. (Eds) *Medical Optical Tomography: Functional Imaging and Monitoring* (Bellingham: SPIE, 1993) **IS11**
2. Rinneberg H, in *The Inverse Problem* (Ed. H Lübbig) (Berlin: Akademic Verlag, 1995) p. 107
3. Tuchin V V (Ed.) *Selected Papers on Tissue Optics: Applications in Medical Diagnostics and Therapy* (Bellingham: SPIE, 1994) **MS102**
4. Ivanitskiĭ G R, Kuniskiĭ A S *Issledovanie Mikrostruktury Ob'ektov Metodami Kogerentnoĭ Optiki* (Microstructural Investigations by Coherent Optical Techniques) (Moscow: Nauka, 1989)

5. Priezzhev A V, Tuchin V V, Shubochkin L P *Lazernaya Diagnostika v Biologii i Meditsine* (Laser Diagnostics in Biology and Medicine) (Moscow: Nauka, 1989)
6. Tuchin V V *J. Laser Applications* (Laser Institute of America) **5** 43 (1993)
7. Tuchin V V *Laser Physics* **3** 767, 925 (1993)
8. Freund D E, McCally R L, Farrell R A *J. Opt. Soc. Am. A* **3** 1970 (1986)
9. Smith T B *J. Mod. Opt.* **35** 93 (1988)
10. Preuss L E, Profio A E (Eds) Special issue on tissue optics *Appl. Opt.* **28** 2207 (1989)
11. Special issue on lasers in biology and medicine IEEE *J. Quantum Electron.* **20** 1342 (1984); **23** 1701 (1987); **26** 2146 (1990)
12. Welch A J, van Gemert M C J (Eds) *Tissue Optics* (New York: Academic, 1992)
13. Motamedi M (Ed.) Special issue on photon migration in tissue and biomedical applications of lasers *Appl. Opt.* **32** 367 (1993)
14. Anderson R R, Parrish J A, in *The Science of Photomedicine* (Eds J D Regan, J A Parrish) (New York: Plenum, 1982)
15. Dillon J *J. Photochem. Photobiol. B: Biol.* **10** 23 (1991)
16. Maksimova I L, Tuchin V V, Shubochkin L P *Opt. Spektrosk.* **60** 801 (1986) [*Opt. Spectrosc.* **60** 493 (1986)]
17. Maksimova I L, Tuchin V V, Shubochkin L P *Opt. Spektrosk.* **65** 615 (1988) [*Opt. Spectrosc.* **65** 365 (1988)]
18. Korolevich A N, Khairulina A Ya, Shubochkin L P *Opt. Spektrosk.* **68** 403 (1990)
19. Schmitt J M, Gandjbakhche A H, Bonner R F *Appl. Opt.* **31** 6535 (1992)
20. MacKintosh F C et al. *Phys. Rev.* **40** 9342 (1989)
21. Gorodnichev E E, Rogozkin D B *Zh. Eksp Teor. Fiz.* **107** 209 (1995) [*JETP* **80** 112 (1995)]
22. Golubentsev A A *Zh. Eksp. Teor. Fiz.* **86** 47 (1984) [*Sov. Phys. JETP* **59** 26 (1984)]
23. Yoo K M et al. *Phys. Rev. A* **39** 3728 (1989)
24. Rytov S M, Kravtsov Yu A, Tatarsky V I *Vvedenie v Statisticheskuyu Radiofiziku* (Introduction to Statistical Radiophysics) (Moscow: Nauka, 1978)
25. Tuchin V V (Ed.) *Coherence — Domain Methods in Biomedical Optics* (Bellingham: SPIE, 1996) **2732**
26. Cummins H Z, Pike E R (Eds) *Photon Correlation and Light Beating Spectroscopy* (New York: Plenum Press, 1974)
27. Cummins H Z, Pike E R (Eds) *Photon Correlation Spectroscopy and Velocimetry* (New York: Plenum, 1977)
28. Kao M H, Yodh A G, Pine D J *Phys. Rev. Let.* **70** 242 (1993)
29. Kaplan P D et at. *Phys. Rev. E* **50** 4827 (1994)
30. Briers J D *Prog. Quant. Electr.* **17** 167 (1993); Briers J D, Webster S *J Biomedical Opt.* **1** 174 (1996)
31. Beauvoit B et al., in *Proc. SPIE* **2326** 127 (1994)
32. Yoon G et al. *IEEE J. Quant. Electron.* **23** 1721 (1987)
33. Tuchin V V (Ed.) *Cell and Biotissue Optics: Applications in Laser Diagnostics and Therapy* (Bellingham: SPIE, 1994) **2100**
34. Duck F A *Physical Properties of Tissue: a Comprehensive Reference Book* (London: Academic Press, 1990)
35. Müller G, Sliney D H (Eds) *Dosimetry of Laser Radiation in Medicine and Biology* (Bellinghan: SPIE, 1989) **IS5**
36. Chance B (Ed.) *Photon Migration in Tissue* (New York: Plenum, 1989)
37. Frank K, Kessler M (Eds) *Quantitative Spectroscopy in Tissue* (Frankfurt am Main: pmi Verlag, 1992)
38. Henderson B W, Dougherty T J (Eds) *Photodynamic Therapy: Basic Principles and Clinical Applications* (New York: Dekker, 1992)
39. Tuchin V V (Ed.) *Optical Methods of Biomedical Diagnostics and Therapy* (Bellingham: SPIE, 1992) **1981**
40. Müller G, Roggan A (Eds) *Laser-Induced Interstitial Thermotherapy* (Bellingham: SPIE, 1995)
41. Chandrasekar S *Radiation Energy Transfer* [Translated into Russian (Moscow: IL, 1953)]
42. Ishimaru A *Propagation and Scattering of Waves in Randomly-Inhomogeneous Media* [Translated into Russian (Moscow: Mir, 1981)]
43. Germogenova T A *Lokal'nie Svoĭstva Reshenĭ Uravneniya Perenosa* (Local Properties of Solutions of Transfer Equations) (Moscow: Nauka, 1986)
44. Ishimaru A *Appl. Opt.* **28** 2210 (1989)
45. Farrell T J, Patterson M S, Wilson B C *Med. Phys.* **19** 879 (1992)
46. Keijzer M, Star W M, Storchi P R M *Appl. Opt.* **27** 1820 (1988)
47. Yoon G, Prahl S A, Welch A J *Appl. Opt.* **28** 2250 (1989)
48. Yoo K M, Liu F, Alfano R R *Phys. Rev. Lett.* **64** 2647 (1990)
49. Dayan I, Havlin S, Weiss G H *J. Modern Opt.* **39** 1567 (1992)
50. Boas D A et al. *Proc. SPIE* (1995) **2389**
51. Motamedi M et al. *J. Appl. Opt.* **28** 2230 (1995)
52. Arridge S R et al. *Med. Phys.* **20** 299 (1993)
53. Tuchin V V, Utz S R, Yaroslavsky I V *Opt. Eng.* **33** 3178 (1994)
54. Ermakov S M, Mikhaĭlov G A *Kurs Statisticheskogo Modelirovaniya* (Textbook of Statistical Modelling) (M: Nauka, 1982)
55. Sobol' I M *Chislennye Metody Monte Karlo* (Numerical Monte Carlo Methods) (Moscow: Nauka, 1973)
56. Wilson B C, Adam G *Med. Phys.* **10** 824 (1983)
57. Keijzer M et al. *Lasers Surg. Med.* **9** 148 (1989)
58. Yaroslavskiĭ I V, Tuchin V V *Opt. Spektrosk.* **72** 934 (1992)
59. Graaff R et al. *Appl. Opt.* **32** 426 (1993)
60. Jacques S L, Wang L-H, in *Optical-Thermal Response of Laserirradiated Tissue* (Eds A J Welch, M J C van Gemert) (New York: Plenum Press., 1995) p. 73
61. Wang L, Jacques S L, Zheng L *Computer Methods and Programs in Biomed.* **47** 131 (1995)
62. Flock S T et al. *IEEE Trans. Biomed. Eng.* **36** 1162 (1989)
63. Wang L-H, Jacques S L *J. Opt. Soc. Am. A* **10** 1746 (1993)
64. Van Gemert M J C et al. *IEEE Trans. Biomed. Eng.* **36** 1146 (1989)
65. Jacques S L, Prahl S A *Lasers Surg. Med.* **6** 494 (1987)
66. Jacques S L, in *Lasers in Dermatology* (Berlin: Springer-Verlag, 1991) p. 1
67. Van Gemert M J C et al. *Lasers Life Sci.* **2** 1 (1988)
68. Bruls W A, van der Leun J C *Photochem. Photobiol.* **40** 231 (1984)
69. Tuchin V V, Utz S R, Yaroslavsky I V, in *Medical Optical Tomography: Functional Imaging and Monitoring* (Eds G Müller et al.) (Bellingham: SPIE, 1993) **IS11** p. 234
70. Schmitt J M et al. *J. Opt. Soc. Am. A* **7** 2141 (1990)
71. Graaff R et al. *Appl. Opt.* **32** 435 (1993)
72. Everett M A et al. *Photochem. Photobiol.* **5** 533 (1966)
73. Keijzer M, Pickering J M, Van Gemert M J C *Laser Surg. Med.* **11** 601 (1991)
74. Svaasand L O et al. *Lasers Med. Sci.* **10** 55 (1995)
75. Kienle A, Hibst R *Phys. Med. Biol.* **40** 1559 (1995)
76. Shcherbakov Yu N et al. *Opt. Spektrosk.* **76** 851 (1994)
77. Tuchin V V et al., in *Laser-Induced Interstitial Thermotherapy* (Bellingham: SPIE, 1995) p.100
78. Star W M, Wilson B C, Patterson M S, in *Photodynamic Therapy, Basic Principles and Clinical Applications* (Eds B W Henderson, T J Dougherty) (New York: Marcel Dekker, 1992) p. 335
79. Van Gemert M J C et al. *Lasers Surgery Med.* **16** 147 (1995)
80. Cheong W F, Prahl S A, Welch A J *IEEE J. Quantum Electron.* **26** 2166 (1990)
81. Wilson B C, Patterson M S, Flock S T *Photochemistry and Photobiology* **46** 601 (1987)
82. Anderson R R, Parrish J A *J. Invest. Dermatology* **77** 13 (1981)
83. Groenhuis R A J, Ten Bosch J J, Ferwerda H A *Appl. Opt.* **22** 2456 (1983)
84. Groenhuis R A J, Ten Bosch J J, Ferwerda H A *Appl. Opt.* **22** 2463 (1983)
85. Hammer M et al. *Phys. Med. Biol.* **40** 963 (1995)
86. Star W M *Phys. Med. Biol.* **40** 1 (1995)
87. Hourdakis C J, Perris A *Phys. Med. Biol.* **40** 351 (1995)
88. Prahl S A, Van Gemert M J C, Welch A J *Appl. Opt.* **32** 559 (1993)
89. Marquet P et al. *Opt. Engineering* **34** 2055 (1995)
90. Bevilacqua F et al. *Opt. Engineering* **34** 2064 (1995)
91. Yaroslavsky I V, Tuchin V V, in *Cell and Biotissue Optics: Applications in Laser Diagnostics and Therapy* (Bellingham: SPIE, 1994) **2100** p. 57
92. Marchesini R et al. *Appl. Opt.* **28** 2318 (1989)
93. Jacques S L, Alter C A, Prahl S A *Lasers Life Sci.* **1** 309 (1987)
94. Yaroslavskaya A N et al. in *Cell and Biotissue Optics: Applications in Laser Diagnostics and Therapy* (Bellingham: SPIE, 1994) **2100** p. 38
95. Flock S T, Wilson B C, Patterson M C *Med. Phys.* **14** 835 (1987)
96. Wilson B C, Patterson M S, Burns D M *Lasers Med. Sci.* **1** 235 (1986)

97. Seyfried M, in *Radiation Measurement in Photobiology* (New York: Academic Press, 1989) p. 191
98. Van de Hulst H C *Multiple Light Scattering* (New York: Academic Press, 1980) **1**
99. Jacques S L, Prahl S A *Lasers Surg. Med.* **6** 494 (1987)
100. Roggan A et al., in *Cell and Biotissue Optics: Applications in Laser Diagnostics and Therapy* (Bellingham: SPIE, 1994) **2100** p. 42
101. Pickering J W et al. *J. Opt. Soc. Am. A* **9** 621 (1992)
102. Pickering J W et al. *Appl. Opt.* **32** 399 (1993)
103. Rol P et al. *Laser Light Ophthal.* **3** 201 (1990); Rol P *Diss. Doctor Natural Sciences* (Zürich: Inst. Biomedical Engineering, 1992)
104. Graaff R et al. *Appl. Opt.* **31** 1370 (1992)
105. Van der Zee P, in *Medical Optical Tomography: Functional Imaging and Monitoring* (Bellingham: SPIE, 1993) **IS11** p. 166
106. Fine I, Lowinger E, Weinreb A, Weinberger D *Phys. Med. Biol.* **30** 565 (1985)
107. van der Hulst T *Light Scattering by Small Particles* (Translated into Russian) (Moscow: Inostrannaya literatura, 1961)
108. Rvachev V P *Metody Optiki Svetorasseivayushchikh Sred v Fizike i Biologii* (Methods of Light-Scattering Media Optics in Physics and Biology) (Minsk: BGU, 1978)
109. Toporets A S *Optika Sherokhovatykh Poverkhnosteĭ* (Optics of Rough Surfaces) (Moscow: Mashinostroenie, 1988)
110. Lopatin V N, Sid'ko F Ya *Vvedenie v Optiku Vzveseĭ Kletok* (Introduction to Cell Suspension Optics) (Novosibirsk:Nauka, 1988)
111. Wang L, Jacques S L *Appl. Opt.* **34** (1995)
112. Bolin F P et al. *Appl. Opt.* **28** 2297 (1989)
113. Shumilina S F *Izv. Akad. Nauk BSSR. Ser. Fiz.-mat. Nauk* (1) 79 (1984)
114. Grisimov V N *Opt. Spektrosk.* **77** 272 (1994) [*Opt. Spectrosc.***77** 245 (1994)]
115. Tuchin V V *Izv. Akad. Nauk SSSR. Ser. Fiz. Nauk* **59** 130 (1995)
116. Ivanov A P, Makarevich S A, Khaĭrullina AYu *ZhPS* **47** 662 (1987)
117. Askar'yan G A *Kvantovaya Elektron.* **9** 1379 (1982) [*Sov. J. Quantum Electron.* **12** 877 (1982)]
118. Askar'yan G A *Pis'ma Zh. Tekh. Fiz.* **9** 311 (1983) [*Sov. Tech. Phys. Lett.* **9** 135 (1983)]
119. Schwarzmaier H - J et al. *Opt. Engineering* **31** 1436 (1992)
120. Cilesiz I F, Welch A J *Appl. Opt.* **32** 477 (1993)
121. Dhadwal H S, Ansari R R, Dellavecchia M A *Opt. Engineering* **32** 233 (1993)
122. Skobelkin O K (Ed.) *Lasery v Khirurgii* (Laser Surgery) (Moscow: Meditsina, 1989)
123. Maksimova I L, Tuchin V V, Shubochkin L P, in *Lazernye Puchki* (Laser Beams) (Khabarovsk: Khab. politekhn. inst., 1985) p. 91
124. Bakutkin V V et al. *ZhPS* **46** 104 (1987) [*J. Appl. Spectrosc.* **46** 86 (1987)]
125. Pierscionek B J *Biomed. Opt.* **1** 147 (1996)
126. Kolmel K F, Sennhenn B, Giese K *British J. Dermatology* **122** 209 (1990)
127. Vladimirov Yu A, Potapenko A Ya *Fiziko-khimicheskie Osnovy Fotobiologicheskikh Protsessov* (Physico-Chemical Basis of Photobiological Processes) (Moscow: Vysshaya shkola, 1989)
128. Sterenborg H J C M, van der Leun J C *Photodermatology* **5** 71 (1988)
129. Splinter R et al. *Lasers Med. Sci.* **8** 15 (1993)
130. Chance B et al. *Analitical Biochemistry* **227** 351 (1995); Liu H et al. *Biomedical Optics* **1** 200 (1996)
131. Maier J S et al. *Opt. Lett.* **19** 2062 (1994)
132. Kohl M et al. *Opt. Lett.* **19** 2170 (1994)
133. Veretout F, Delaye M, Tardieu A *J. Molecular Biology* **205** 713 (1989)
134. Steinke J M, Shepherd A P *J. Opt. Soc. Am. A* **5** 813 (1988)
135. Gregorzewski B, Syroczynsky M, Pyskir M, in *Proc. SPIE* **2340** 487 (1995)
136. Zimnyakov D A et al., in *Proc. SPIE* **2673** 44 (1996)
137. Sinichkin Yu P, Utz S R, Pilipenko E A *Opt. Spektrosk.* **80** 260 (1996)
138. Minin I N *Teoriya Perenosa Izlucheniya v Atmosfere Planet* (Radiative Transfer Theory for Planetary Atmosphere) (Moscow: Nauka, 1988)
139. Yoo K M et al., in *Medical Optical Tomography: Functional Imaging and Monitoring* (Bellingham: SPIE, 1993) **IS11** p. 425
140. Berg R, Andersson-Engels S, Svanberg S, in *Medical Optical Tomography: Functional Imaging and Monitoring* (Bellingham: SPIE, 1993) **IS11** p. 397
141. Patterson M S, Chance B, Wilson B C *Appl. Opt.* **28** 2331 (1989)
142. Jacques S L *IEEE Trans. Biomed. Engineering* **36** 1155 (1989)
143. Delpy D T et al. *Phys. Med. Biol.* **33** 1433 (1988)
144. Cui W, Wang N, Chance B *Opt. Lett.* **16** 1632 (1991)
145. Ferrari M et al. *J. Photochemistry Photobiology B: Biology* **16** 141 (1992)
146. Liu P, Kruger R A *Opt. Engineering* **33** 2783 (1994)
147. de Haller E B, Depeursinge C *Med. Biol. Eng. Comp.* **31** 165 (1993)
148. Andersson-Engels S, Berg R, Svanberg S *Opt. Lett.* **15** 1179 (1990)
149. Wang L et al. *Science* **253** 769 (1991)
150. Das B B, Yoo K M, Alfano R R *Optics Lett.* **18** 1092 (1993)
151. Lyubimov V V *Opt. Spektrosk.* **76** 814 (1994) [*Opt. Spectrosc.***76** 725 (1994)]
152. Barbour R L et al., in *Proc. SPIE* **1641** 21 (Bellingham: SPIE, 1992)
153. Yoo K M, Liu F, Alfano R R *J. Opt. Soc. Am. B.* **7** 1685 (1990)
154. Yodh A, Chance B *Physics Today* March 34 (1995)
155. Arridge S R, Cope M, Delpy D T *Phys. Med. Biol.* **37** 1531 (1992)
156. Yaroslavsky I V, Tuchin V V *BRAS Physics/Suppl. Physics of Vibrations* **58** (4) (1994)
157. Haskell R C et al. *J. Opt. Soc. Am. A* **11** 2727 (1994)
158. Tromberg B J et al. *Appl. Opt.* **32** 607 (1993)
159. O'Leary M A et al. *Phys. Rev. Lett.* **69** 2658 (1992)
160. Boas D A et al. *Phys. Rev. E* **47** R 2999 (1993)
161. Boas D A et al. *Proc. Nat. Acad. Sci. USA* **91** 4887 (1994)
162. Lakowicz J R, Berndt K *Chem. Phys. Lett.* **166** 246 (1990)
163. Patterson M S et al. *Appl. Opt.* **30** 4474 (1991)
164. Schmitt J M, Knüttel A, Knutson J R *J. Opt. Soc. Am. A* **9** 1832 (1992)
165. Fishkin J B, Gratton E *J. Opt. Soc. Am. A* **10** 127 (1993)
166. Svaasand L O et al. *Opt.Engineering* **32** 258 (1993)
167. Mazurenko Yu T *Opt. Spektrosk.* **76** 816 (1994) [*Opt. Spectrosc.* **76** 727 (1994)]
168. Sevick E M el al., in *Medical Optical Tomography: Functional Imaging and Monitoring* (Bellingham: SPIE, 1993) **IS11** p. 485
169. Patterson M S, Pogue B W, Wilson B C, in *Medical Optical Tomography: Functional Imaging and Monitoring* (Bellingham: SPIE, 1993) **IS11** p. 513
170. Gratton E, Maier J in *Medical Optical Tomography: Functional Imaging and Monitoring* (Bellingham: SPIE, 1993) **IS11** p. 534
171. Chance B, Liu H, Kang K, in *Medical Optical Tomography: Functional Imaging and Monitoring* (Bellingham: SPIE, 1993) **IS11** p. 545
172. Chance B *Annual Rev. Biophysics Biophys. Chem.* **20** 1 (1991)
173. Pogue B W, Patterson M S *Phys. Med. Biol.* **39** 1157 (1994)
174. Pogue B W et al. *Phys. Med. Biol.* **40** 1709 (1995)
175. Yaroslavsky I V et al., in *Proc. SPIE* **2326** 465 (Bellingham: SPIE, 1995)
176. Yaroslavsky I V et al., in *Proc. SPIE* **2626** 06 (Bellingham: SPIE, 1995)
177. Tuchin V V *Metody Izmereniya Parametrov Volokonnikh Svetovodov* (Methods for Measuring Optical Fiber Parameters) (Moscow: TsNII Elektronika, 1987)
178. Zharov V P, Letokhov V S *Lazernaya Optiko-Akusticheskaya Spektroskopiya* (Laser Opto-Acoustic Spectroscopy) (Moscow: Nauka, 1984) [Translated into English (Berlin: Springer-Verlag, 1986)]
179. O'Leary M A et al., in *OSA Proc. on Advances in Optical Imaging and Proton Migration* (Ed. R R Alfano) **21** 106 (1994)
180. Knuttel A, Schmitt J M, Knutson J R *Appl. Opt.* **32** 381 (1993)
181. Fantini S , Franceschini M A, Gratton E *J. Opt. Soc. Am. B* **11** 2128 (1994)
182. Moon J A, Reintjes J *Opt. Lett.* **19** 521 (1994)
183. Morgan S P, Khong M P, Somekh M G, in *Proc. SPIE* **2626** 32 (1995)
184. Svaasand L O, Gomer Ch J, in *Dosimetry of Laser Radiation in Medicine and Biology* (Bellinghan: SPIE, 1989) p. 114
185. Jacques S L et al., in *Proc. SPIE* **2671** 43 (1996); Ostermeyer M R et al., in *OSA TOPS on Biomedical Optical Spectroscopy and Diagnostics* **3** 20 (1996)
186. Bicout D et al. *Phys. Rev. E* **49** 1767 (1994)

187. Maksimova I L, Tatarintsev S N, Shubochkin L P *Opt. Spektrosk.* **72** 1171 (1992)
188. Bruscaglioni P, Zaccanti G, Wei Q *Appl. Opt.* **32** 6142 (1993)
189. Loiko V A, Molochko V I *Opt. Spektrosk.* **79** 329 (1995) [*Opt. Spectrosc.* **79** 304 (1995)]
190. Korolevich A N, Khairullina A Ya, Shubochkin L P *Opt. Spektrosk.* **77** 278 (1994) [*Opt. Spectrosc.* **77** 251 (1994)]
191. Dolginov A Z, Gnedin Yu M, Silant'ev N A *Rasprostranenie i Polyarizatsiya Izlucheniya v Kosmicheskoĭ Srede* (Distribution and Polarization of Radiation in the Outerspace) (Moscow: Nauka, 1979)
192. Eliyahu D, Rosenbluch M, Freund I *J. Opt. Soc. Am. A* **10** 477 (1993)
193. Zege E P, Chaikovskaya L I *ZhPS* **44** 996 (1986) [*J. Appl. Spectrosc.* **44** 655 (1986)]
194. Kuga Y, Ishimaru A, Ma Q *Radio Sci.* **24** 247 (1989)
195. Val'kov A Yu, Romanov V P, Shalaginov A N *Usp. Fiz. Nauk* **164** 149 (1994) [*Phys. Usp.* **37** 139 (1994)]
196. Kuz'min V L, Romanov V P *Usp. Fiz. Nauk* **166** 247 (1996) [*Phys. Usp.* **39** 231 (1996)]
197. Hielscher A H, Mourant J R, Bigio I J, in *OSA TOPS on Biomedical Optical Spectroscopy and Diagnostics* **3** 26 (1996)
198. Yaroslavsky A N et al., in *Proc. SPIE* **2678C** 34 (Bellingham: SPIE, 1996)
199. Anderson R R *Archives Dermatology* **127** 1000 (1991)
200. Boren K, Hafmen D *Absorption and Scattering of Light by Small Particles* [Translated into Russian (Moscow: Mir, 1986)]
201. Johnston R G, Singham S B, Salzman G C, in *Comments Mol. Cell. Biophys.,Comments Mod. Biol. A* **5** 171 (1988)
202. Salzman G C et al., in *Flow Cytometry and Sorting* (New York: Wiley-Liss,1990) **81**
203. Bettelheim F A *The Ocular Lens. Structure, Function and Pathology* (New York: Marcel Dekker, 1985)
204. Farrell R A, Freund D E, McCally R L, in *Mat. Res. Soc. Symp. Proc.* **255** 233 (1992)
205. Farrell R A, Freund D E, McCally R L *Johns Hopkins APL Technical Digest* **11** 191 (1990)
206. Maksimova I L, Shubochkin L P *Opt. Spektrosk.* **70** 1276 (1991)
207. Tuchin V V et al., in *Proc. SPIE* **2393** 237 (1995); Tuchin V V et al., in *Proc. SPIE* **2126** 393 (Bellingham: SPIE, 1994)
208. Zigman S, Sutliff G, Rounds M *Lens and Eye Toxicity Research* **8** 259 (1991)
209. Tuchin V V et al., in *Proc SPIE* **2925** 16 (Bellingham: SPIE, 1996)
210. Priezzhev A V, Tuchin V V, Shubochkin L P *Izv. AN SSSR. Ser. Fiz.* **53** 1490 (1989)
211. Maksimova I L et al. *Izv. AN SSSR. Ser. Fiz.* **54** 1918 (1990)
212. Maksimova I L Diss. kand. fiz-mat. nauk (Saratov: Saratovsk. Univer., 1991)
213. Shubochkin A P Diss. kand. fiz-mat. nauk (Saratov: Saratovsk. Univer., 1987)
214. Shubochkin L P, Tuchin V V, in *Proc. SPIE* **1403** 720 (Bellingham: SPIE, 1990)
215. Dreher A W, Reiter K *Clin. Vis. Sci.* **7** 481 (1992)
216. Guseva N P et al., in *Proc. SPIE* **1403** 332 (Bellingham: SPIE, 1990)
217. Van De Merwe W P, Huffman D R, Bronk B V *Appl. Opt.* **28** 5052 (1989)
218. Bronk B V, Van De Merwe W P, Stanley M *Cytometry* **13** 155 (1992)
219. Bronk B V et al., *Biophysical J.* **69** 1170 (1995)
220. de Grooth B G et al. *Cytometry* **8** 539 (1987)
221. Poupinet L, Jarry G *J. Optics* (Paris) **24** 279 (1993)
222. Fercher A F et al. *Opt. Commun.* **117** 43 (1995); Fercher A F *J. Biomed. Opt.* **1** 157 (1996)
223. Gelikonov V M et al. *Pis'ma Zh. Teor. Eksp. Fiz.* **61** 149 (1995) [*JETF Lett.* **61** 158 (1995)]
224. Masters B R (Ed.) *Noninvasive Diagnostics Techniques in Ophthalmology* (New York: Springer-Verlag, 1990)
225. Wilson T (Ed.) *Confocal Microscopy* (London: Academic Press, 1990)
226. Masters B R, Thaer A A *Appl. Opt.* **33** 695 (1994)
227. Rajadhyaksha M M et al., in *Proc. SPIE* **2671** 44 (Bellingham: SPIE, 1996)
228. Masters B *J. Biomed. Opt.* **1** (1996)
229. Kimura Y et al., in *Proc. SPIE* **2672** 12 (Bellingham: SPIE, 1996)
230. Ul'yanov S S, Ryabukho V P, Tuchin V V *Opt. Engineering* **33** 908 (1994)
231. Ul'yanov S S, Zimnyakov D A, Tuchin V V *Opt. Engineering* **33** 3189 (1994)
232. Romanovskiĭ Yu M, Teplov V A *Usp. Fiz. Nauk* **165** 555 (1995) [*Phys. Usp.* **38** 521 (1995)]
233. Zhevandrov N D *Usp. Fiz. Nauk* **165** 1193 (1995) [*Phys. Usp.* **38** 1147 (1995)]